Article

TRANSPARENT PROCESS

EMBO reports

Myogenin promoter-associated lncRNA *Myoparr* is essential for myogenic differentiation

Keisuke Hitachi[1], Masashi Nakatani[1], Akihiko Takasaki[2], Yuya Ouchi[3], Akiyoshi Uezumi[1,†], Hiroshi Ageta[1], Hidehito Inagaki[3], Hiroki Kurahashi[3] & Kunihiro Tsuchida[1,*]

Abstract

Promoter-associated long non-coding RNAs (lncRNAs) regulate the expression of adjacent genes; however, precise roles of these lncRNAs in skeletal muscle remain largely unknown. Here, we characterize a promoter-associated lncRNA, *Myoparr*, in myogenic differentiation and muscle disorders. *Myoparr* is expressed from the promoter region of the mouse and human *myogenin* gene, one of the key myogenic transcription factors. We show that *Myoparr* is essential both for the specification of myoblasts by activating neighboring *myogenin* expression and for myoblast cell cycle withdrawal by activating myogenic microRNA expression. Mechanistically, *Myoparr* interacts with Ddx17, a transcriptional coactivator of MyoD, and regulates the association between Ddx17 and the histone acetyltransferase PCAF. *Myoparr* also promotes skeletal muscle atrophy caused by denervation, and knockdown of *Myoparr* rescues muscle wasting in mice. Our findings demonstrate that *Myoparr* is a novel key regulator of muscle development and suggest that *Myoparr* is a potential therapeutic target for neurogenic atrophy in humans.

Keywords chromatin; DEAD box protein; myogenesis; transcriptional regulation

Subject Categories Development & Differentiation; RNA Biology

DOI 10.15252/embr.201847468 | Received 25 November 2018 | Revised 17 December 2018 | Accepted 19 December 2018 | Published online 8 January 2019

EMBO Reports (2019) 20: e47468

Introduction

Long non-coding RNAs (lncRNAs) are pervasively transcribed from the genome. Intriguingly, most intergenic lncRNAs are derived from cis-regulatory regions, i.e., enhancers and promoters [1]. Enhancer-derived lncRNAs, also known as eRNAs, are generally short, unstable, and bidirectional, and their generation is strongly associated with enhancer activity [2]. Besides the enhancer region, multiple RNA polymerase II (Pol II)-dependent promoters bidirectionally produce coding and non-coding transcripts [3]. Although promoter upstream transcripts (PROMPTs) are rapidly turned over by the RNA exosome [4,5], increasing evidence indicates that promoter-associated anti-sense lncRNAs act in cis to regulate the transcription of neighboring protein-coding genes, particularly as developmental regulators [3,6–8]. However, molecular characterization of these lncRNAs in cell proliferation, differentiation, and diseases remains unexplored.

The differentiation process of skeletal muscle cells, called myogenesis, has been studied as a model of cell differentiation systems. One of the myogenic regulatory factors (MRFs), MyoD, triggers the expression of cyclin-dependent kinase inhibitors to arrest the cell cycle of proliferating myoblasts [9] and also initiates the expression of early skeletal muscle-specific genes including *myogenin*, coding one MRF [10]. Subsequently, MyoD and myogenin promote the entry of myoblasts into the myogenic differentiation lineage through the activation of later skeletal muscle-specific genes [11]. Additionally, muscle-specific microRNAs (miRNAs) broaden the regulatory networks of myogenesis by modulating the expression of target genes in myoblast proliferation and differentiation [12]. Thus, induction of muscle-specific genes coordinated with the cell cycle exit at an appropriate time is required for the formation of terminally differentiated skeletal muscle cells.

Myogenin gene is indispensable for skeletal muscle development [13]. The expression of *myogenin* is highly restricted to myogenic tissues in embryonic, fetal, and adult skeletal muscles. However, the mechanisms inducing high-level *myogenin* expression in skeletal muscle cells have not been elucidated. In this study, we identified a novel promoter-associated lncRNA, *Myoparr*, derived from the upstream region of the *myogenin* gene. *Myoparr* was coexpressed with *myogenin* and was essential for the active transcription of *myogenin* in an epigenetic manner. Thus, identification of *Myoparr* uncovered a molecular mechanism required for high-level *myogenin* expression. Besides *myogenin* expression, *Myoparr* was essential to activate the expression of myogenic miRNAs, which control cell cycle withdrawal of myoblasts. In addition, we found that *Myoparr* bound Ddx17, a transcriptional coactivator of MyoD, and promoted the protein–protein interaction between Ddx17 and histone acetyltransferase PCAF, indicating that *Myoparr* functions by binding with transcriptional activator during myogenesis. Furthermore, we

1 Division for Therapies against Intractable Diseases, Institute for Comprehensive Medical Science (ICMS), Fujita Health University, Toyoake, Japan
2 Department of Medical Technology, School of Health Sciences, Gifu University of Medical Science, Seki, Japan
3 Genome and Transcriptome Analysis Center, Fujita Health University, Toyoake, Japan
*Corresponding author. Tel: +81 562 93 9384; E-mail: tsuchida@fujita-hu.ac.jp
†Present address: Department of Geriatric Medicine, Tokyo Metropolitan Institute of Gerontology, Tokyo, Japan

identified the human *Myoparr* counterpart from human primary skeletal muscle cells and provided *in vivo* evidence that *Myoparr* knockdown (KD) blocked neurogenic atrophy in mice. Thus, our study not only reveals a new role of promoter-associated lncRNAs in cell proliferation and differentiation but also provides insight into human regenerative medicine targeting promoter-associated lncRNAs.

Results

Identification and characterization of a *myogenin* promoter-associated lncRNA, *Myoparr*, in skeletal muscle cells

Although the proximal 133 bp of the *myogenin* promoter region is sufficient to define its spatiotemporal expression, up to 1.5 kb of upstream region is required for high-level *myogenin* expression in mouse skeletal muscle [14]. Publicly available chromatin immunoprecipitation (ChIP) sequencing (ChIP-seq) data showed the occupancy of Pol II around this locus in terminally differentiated myotubes (Fig 1A), suggesting that the upstream region of *myogenin* is transcriptionally active. Thus, we performed reverse transcription polymerase chain reaction (RT–PCR) to ascertain whether this region is actively transcribed in C2C12 myotubes and detected previously unidentified transcripts in an RT-dependent manner in at least four different regions (Fig 1B). Subsequent strand-specific RT–PCR using total and poly(A)+ RNAs showed the presence of polyadenylated anti-sense and sense transcripts in the upstream region of *myogenin* (Fig 1C).

Both full-length transcripts were determined by rapid amplification of cDNA ends (RACE) analyses. The 5′- and 3′-RACE of the anti-sense transcript revealed a single exon transcript, expressed from the upstream region (−243 to −1414) of the *myogenin* gene (Fig EV1A). The transcription start site of *myogenin* was positioned as +1. On the other hand, the 5′- and 3′-RACE of the sense transcript revealed the presence of multiple 5′- and 3′-ends initiated from 2.5 to 2.8 kb upstream of the *myogenin* gene (Fig EV1A). Relatively weak sense transcript detected by the strand-specific RT–PCR would be due to intron-derived sequences. Although the 3′-ends of the sense transcripts mainly overlapped with *myogenin* mRNA, sequences encoding the initiating methionine of *myogenin* were lost in almost every sense transcript examined.

The nuclear/cytoplasmic expression of both transcripts was quantified by quantitative PCR (qPCR) in differentiating C2C12 cells. As compared to protein-coding RNAs such as *myogenin* and *GAPDH*, both anti-sense and sense transcripts were concentrated in the nuclei as with *Neat1* non-coding RNA (Fig 1D). *In silico* analyses of protein-coding potential predicted that both transcripts are non-coding RNAs (Fig EV1B). Indeed, no translated proteins from either transcript were detected *in vitro*, whereas *EGFP* and *myogenin* generated corresponding proteins (Fig EV1C). From these results, we concluded that both transcripts are putative non-coding RNAs. Therefore, we referred to the anti-sense transcript as a *myo*genin promoter-associated myogenic regulatory anti-sense long non-coding RNA (*Myoparr*) and the sense transcript as *myogenin*-associated sense long non-coding RNA.

Full-length *Myoparr* (1,172 nt from C2C12 myotubes and 1,167 nt from murine skeletal muscle) was detected and cloned by PCR. *Myoparr* contains a potential RNA nuclear retention signal [15] at the 5′-side, a putative polyadenylation signal 15-nt upstream of the poly(A) tail, and a LINE-1-like sequence in the 3′-half (Fig EV1D). In C2C12 myotubes, *Myoparr* was more enriched in chromatin pellet extract (CPE) than in soluble nuclear extract (SNE) as with *Malat1*, which associates with chromatin [16] (Fig 1E), suggesting that the presence of *Myoparr* as chromatin-enriched RNA affects the expression of neighboring genes [17]. We successfully detected an anti-sense transcript at the upstream region of *myogenin* in human primary myotubes (Fig EV1E and F) and determined that the 5′- and 3′-ends of the transcript corresponded to the human counterpart of *Myoparr* by RACE analyses (Fig EV1G). Genomic localization of both mouse and human *Myoparr* is shown in Appendix Fig S1A and B and listed in Appendix Table S1. In this study, we further examined the role of *Myoparr* in myogenic cell proliferation and differentiation through the activation of *myogenin* expression.

The expression of *Myoparr* and *myogenin* is mutually correlated and regulated by MyoD and TGF-β

We first examined the expression pattern of *Myoparr* during skeletal muscle differentiation. Similar to *myogenin* expression, *Myoparr* expression gradually increased during *in vitro* (C2C12 cells and mouse primary myoblasts) and *in vivo* (mouse embryos) myogenesis (Fig 2A and B). Among embryonic organs, *Myoparr* expression was enriched in skeletal muscle tissue as with *myogenin* expression (Fig EV2A). Absolute quantification assays showed that *Myoparr* is present at 5.0 ± 0.7 copies per cell and *myogenin* is present at $1{,}868.7 \pm 351.1$ copies per cell in differentiating C2C12 cells. Thus, the expression level of *Myoparr* was low compared with that of *myogenin*, in accordance with the expression level of other lncRNAs [18]. We also found that the expression of human *Myoparr* and *myogenin* increased during human myoblast differentiation (Fig EV2B). These results indicated that the expression of *Myoparr* and *myogenin* is mutually correlated during skeletal muscle differentiation in both humans and mouse.

We next examined whether *Myoparr* expression is regulated by MyoD and TGF-β, which control *myogenin* expression positively and negatively, respectively [13,19]. During the conversion of C3H10T1/2 fibroblasts into myogenic cells by MyoD expression, a significant increase in *Myoparr* expression was observed (Fig 2C). In contrast, TGF-β treatment significantly decreased *Myoparr* expression during C2C12 differentiation (Fig 2D), suggesting a common regulatory mechanism underlying *Myoparr* and *myogenin* expression. Since the intergenic region between *Myoparr* and *myogenin* is very short (Fig 2E), we hypothesized that *Myoparr* shares a common promoter with *myogenin*. Accordingly, the intergenic region was cloned, and its transcriptional activities in both directions were measured by luciferase assay. During C2C12 differentiation, this region showed bidirectional promoter activity (Fig 2F); the *Myoparr* promoter activity was a quarter of that of the *myogenin* promoter, whereas the unidirectional *GAPDH* promoter showed no activity in the opposite direction (Fig EV2C). MyoD expression increased both promoter activities in differentiating C2C12 cells (Fig 2F). Introduction of mutations in the E-box elements that are important for responsiveness of MyoD and TGF-β [20] significantly decreased the activation of both promoters

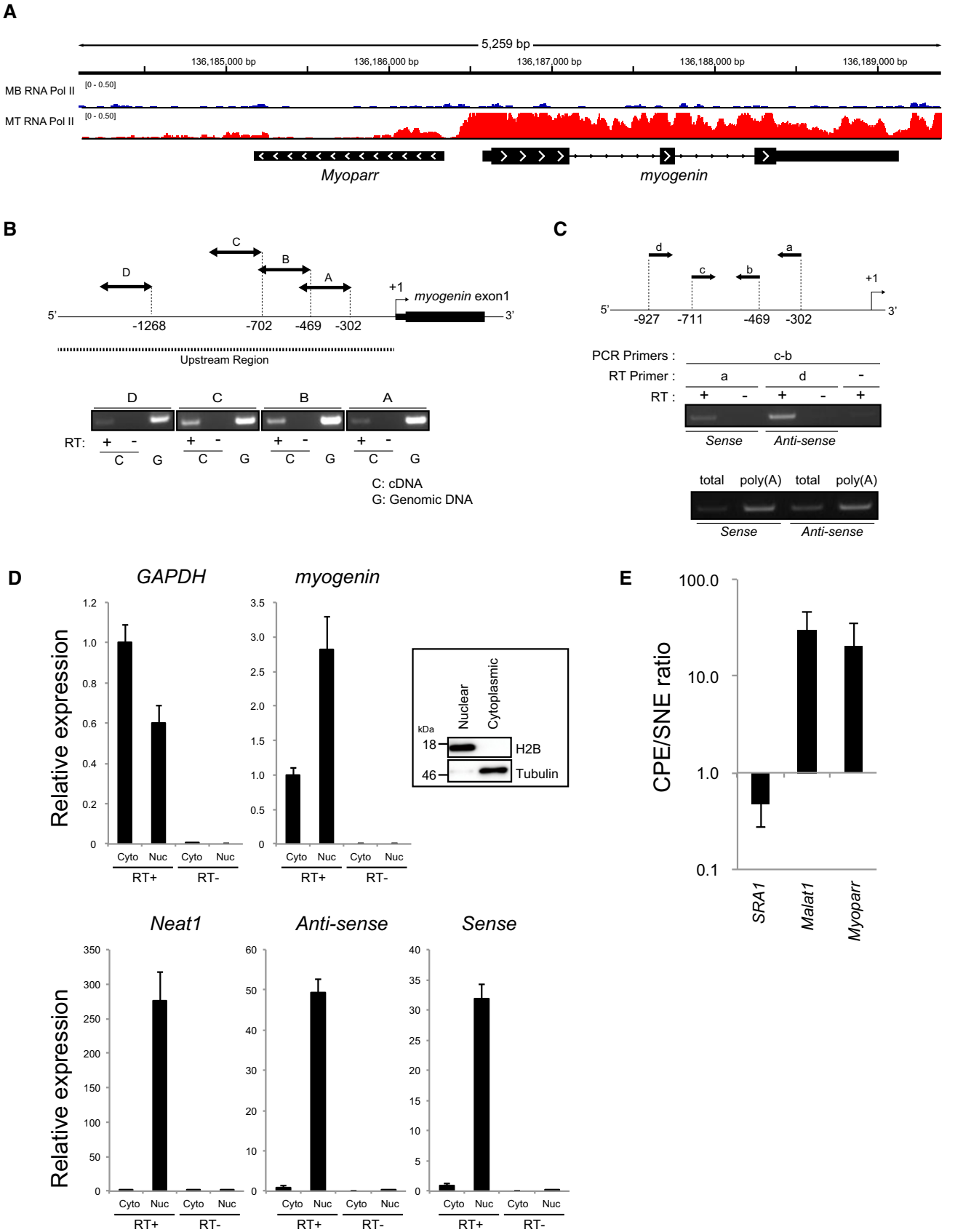
A
5,259 bp
136,185,000 bp
136,186,000 bp
136,187,000 bp
136,188,000 bp
136,189,000 bp
MB RNA Pol II
[0 - 0.50]
MT RNA Pol II
[0 - 0.50]
Myoparr
myogenin
B
C
B
A
D
+1
myogenin exon1
5'
3'
-1268
-702
-469
-302
Upstream Region
D
C
B
A
RT: + - + - + - + -
C G C G C G C G
C: cDNA
G: Genomic DNA
C
d
c
b
a
+1
5'
3'
-927
-711
-469
-302
PCR Primers : c-b
RT Primer : a d -
RT : + - + - +
Sense
Anti-sense
total poly(A) total poly(A)
Sense
Anti-sense
D
GAPDH
myogenin
Relative expression
Cyto Nuc Cyto Nuc
RT+ RT-
Nuclear
Cytoplasmic
kDa
18
H2B
46
Tubulin
Neat1
Anti-sense
Sense
Relative expression
E
CPE/SNE ratio
100.0
10.0
1.0
0.1
SRA1
Malat1
Myoparr

Figure 1.

Figure 1. A promoter-associated lncRNA, *Myoparr*, is expressed from the upstream region of the *myogenin* locus.

A Occupancies of Pol II at the *myogenin* locus in C2C12 myoblasts (MB, shown in blue) and myotubes (MT, shown in red). *Myoparr* is located immediately upstream from the *myogenin* gene.

B Schematic representation of the upstream region of *myogenin* and amplified regions by RT–PCR (top). RT–PCR for the novel transcripts at the upstream region of *myogenin* in C2C12 myotubes (bottom). The presence or absence of reverse transcriptase (RT) is shown by (+) or (−), respectively. The templates (cDNA or genomic DNA) are indicated by C or G, respectively.

C The primers used for RT–PCR (top). Strand-specific RT–PCR for the novel transcripts at the upstream region of *myogenin* in C2C12 myotubes using total RNA (middle and bottom) and poly(A)+ RNA (bottom).

D Relative expression of indicated RNAs in differentiating C2C12 cells. The presence or absence of RT is shown by (+) or (−), respectively. PCR products were verified by sequencing. $n = 3$, mean ± SD. The nuclear/cytoplasmic fractionation is confirmed by the expression of H2B and tubulin, respectively.

E Chromatin pellet extract (CPE)/soluble nuclear extract (SNE) ratio of *SRA1*, *Malat1*, and *Myoparr* in C2C12 myotubes on a log scale. $n = 3$, mean ± SD.

(Fig 2G). TGF-β treatment also decreased both promoter activities (Fig 2H), and mutations in the E-box elements effectively attenuated TGF-β-dependent repression of both promoter activities (Fig 2H). Taken together, these results indicated that common regulatory mechanisms may play a role in the expression of *Myoparr* and *myogenin*.

Myoparr is required for myogenic differentiation through the activation of *myogenin* expression

The strong correlation between *Myoparr* and *myogenin* expression suggested a reciprocal regulation of these genes during myogenesis. To examine whether *Myoparr* is a significant regulator of *myogenin* or only a transcriptional artifact from the bidirectional promoter, we knocked down *Myoparr* using two distinct small interfering RNAs (siRNAs) in differentiating C2C12 cells. The expression of *myogenin* mRNA and protein induced by serum withdrawal was markedly inhibited by *Myoparr* depletion (Fig 3A and B). The same results were observed by anti-sense oligonucleotides (ASOs)-mediated *Myoparr* KD (Fig EV3A–C). On the contrary, *Myoparr* expression was increased by *myogenin* KD (Fig 3C), possibly resulting from genetic compensation and/or feedback regulation. These results suggested that *Myoparr* is not simply a transcriptional artifact, but rather a significant activator of *myogenin* during myogenic differentiation.

To understand the mechanisms involved in *Myoparr*-mediated augmentation of *myogenin* mRNA expression, we assessed the occupancy of Pol II at the *myogenin* locus. ChIP assays revealed that *Myoparr* KD resulted in the reduction of Pol II occupancy at the *myogenin* locus but not at the control *GAPDH* locus (Figs 3D and EV3D). Moreover, *Myoparr* depletion led to significant decreases in H3K4me3 and H3K27ac levels, landmarks of active promoters, at the *myogenin* locus (Fig 3D). Although promoter-associated lncRNAs were previously shown to alter the DNA methylation status [8], *Myoparr* depletion had little effect on DNA methylation of the *myogenin* locus (Fig EV3E–G). To examine whether *Myoparr* directly binds to the *myogenin* promoter region, we performed chromatin isolation by RNA purification (ChIRP) assays with *Myoparr* probes (odd- and even-numbered). We were able to specifically recover endogenous *Myoparr* from differentiating C2C12 cells with *Myoparr* probes, compared with *GAPDH* mRNA as a negative control (Fig 3E). Enrichment of *Myoparr* was not observed with control *LacZ* probes. *Myoparr* probes also enriched the *myogenin* promoter region but not the *myogenin* 3′ untranslated region (UTR) and *GAPDH* promoter in ChIRP assays (Fig 3F), indicating that endogenous *Myoparr* bound to the *myogenin* promoter in differentiating C2C12 cells. Thus, these results indicated that *Myoparr* is required to maintain an active promoter signature around the *myogenin* locus through binding to target chromatin during C2C12 myogenesis.

Given the known roles of *myogenin* in skeletal muscle differentiation, we examined the biological role of *Myoparr* in C2C12 differentiation. At an early phase of myogenic differentiation, *Myoparr* KD significantly decreased the number of myogenin-positive cells (Fig 3G). At a later phase, *Myoparr* KD led to repression of myogenic differentiation as shown by decreased expression of myosin heavy chain (MHC), a late myogenic differentiation marker (Figs 3H and EV3H and I). Moreover, *Myoparr* depletion significantly reduced *MyoD1* expression accompanied with a decline of Pol II occupancy at the *MyoD1* locus (Fig EV3J–M), suggesting that *Myoparr* supports *MyoD1* expression in a positive feedback loop.

To investigate the effect of *Myoparr* depletion more extensively, we compared global gene expression profiles between *Myoparr*- and *myogenin*-depleted C2C12 cells using RNA sequencing (RNA-seq). Statistically significant expression changes were observed in 693 genes (299 up-regulated and 394 down-regulated) by *Myoparr* KD, while the expression levels of 148 genes (23 up-regulated and 125 down-regulated) were significantly altered by *myogenin* KD (Table EV1). The intersection of genes showing significantly different expression in both *Myoparr* and *myogenin* depletion was 25.6-fold greater than that expected by chance ($P = 8.14738 \times 10^{-142}$; Fig 3I and Table EV1), with a positive correlation ($R = 0.63$; Fig 3J). However, the expression of a large number of genes regulated by *Myoparr* was not significantly altered by *myogenin* KD, suggesting that *Myoparr* may also act in a *myogenin*-independent manner. In agreement with this finding, genes up-regulated by *Myoparr* KD were preferentially classified as cell cycle and cell division categories based on Gene Ontology (GO), whereas genes whose expression was down-regulated by *Myoparr* KD or *myogenin* KD were enriched in muscle contraction and muscle development categories (Fig 3K–M and Table EV1). Genes commonly regulated by both *Myoparr* KD and *myogenin* KD (112 genes) were also preferentially classified as muscle contraction and muscle development categories (Fig 3N). Of note, genes up-regulated by *myogenin* KD were not classified. The results of RNA-seq were verified by qPCR of representative genes in each GO category using two independent siRNAs (Appendix Fig S2A–H). From these results, we concluded that *Myoparr* is essential for specification of myoblasts to differentiation lineage through the *Myoparr* (upstream) and *myogenin* (downstream) pathway and that *Myoparr* also likely regulates the cell cycle and cell division pathway in a *myogenin*-independent manner.

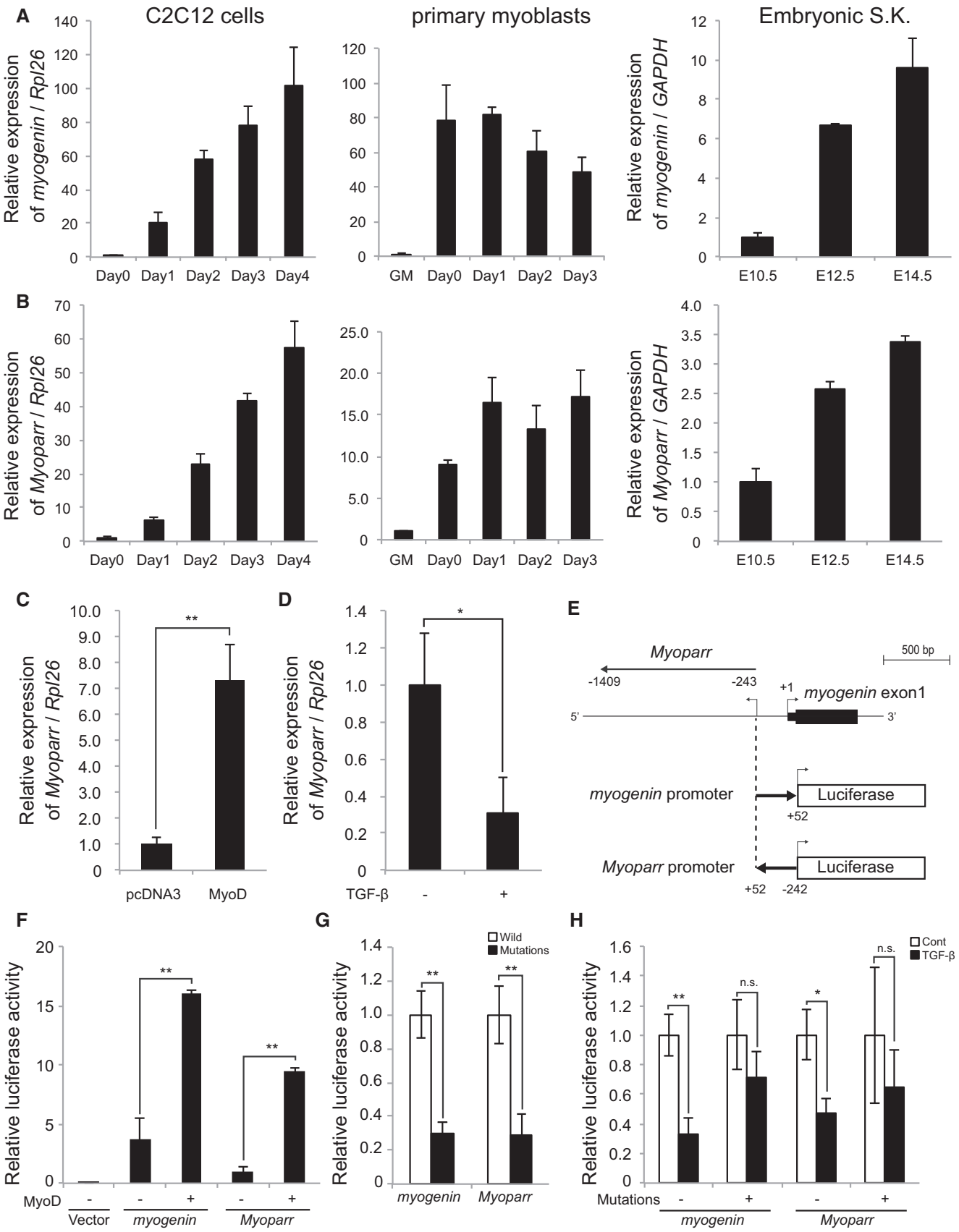

Figure 2.

Figure 2. *Myoparr* expression is correlated with *myogenin* expression and regulated by MyoD and TGF-β.

A, B Quantitative RT–PCR for *myogenin* (A) and *Myoparr* (B) during myogenesis of C2C12 cells, primary mouse myoblasts (growth medium, GM), and mouse embryonic skeletal muscle (S.K.). The *x*-axis shows days after differentiation induction or embryonic days. $n = 3$, mean ± SD.

C qRT–PCR showing increased *Myoparr* expression by MyoD in C3H10T1/2 fibroblasts. $n = 4$, mean ± SD. $^{**}P < 0.01$ (unpaired two-tailed Welch's *t*-test).

D Treatment of recombinant TGF-β for 24 h decreased *Myoparr* expression in differentiating C2C12 cells. $n = 3$, mean ± SD. $^{*}P < 0.05$ (unpaired two-tailed Student's *t*-test).

E Schematic diagram of the constructs used for luciferase assays.

F Relative luciferase activities of the indicated promoter in differentiating C2C12 cells by exogenous MyoD. $n = 3$, mean ± SD. $^{**}P < 0.01$ (unpaired two-tailed Student's *t*-test).

G Relative luciferase activities of the indicated promoter with/without E-box mutations in differentiating C2C12 cells. $n = 3$, mean ± SD. $^{**}P < 0.01$ (unpaired two-tailed Student's *t*-test).

H Relative luciferase activities of the indicated promoter with/without E-box mutations in differentiating C2C12 cells by TGF-β treatment. $n = 3$, mean ± SD. $^{*}P < 0.05$. $^{**}P < 0.01$. n.s., not significant (unpaired two-tailed Student's *t*-test).

Myoparr interacts with DEAD box protein Ddx17 and regulates the protein–protein interaction between Ddx17 and histone acetyltransferase PCAF

The lncRNA–protein interactions influence the expression of neighboring genes [21]; therefore, identifying proteins associated with *Myoparr* is crucial to determine the mechanisms underlying *Myoparr*-mediated transcriptional activation. *Myoparr* labeled with 5-bromouridine (BrU) was mixed with nuclear lysates extracted from C2C12 myotubes. Following immunoprecipitation of *Myoparr* with a BrdU antibody, RNA–protein complexes were competitively eluted with free 5-bromo-2′-deoxyuridine (BrdU). After electrophoresis, protein bands specifically enriched in the *Myoparr* immunoprecipitant compared with the control sample were excised. *Myoparr*-interacting proteins were then analyzed by LC-MS/MS (Fig 4A). We identified Ddx17 (both p72 and p82 isoforms), hnRNPK, and Tial1/TIAR as *Myoparr*-associated proteins (Appendix Fig S3A). Among these proteins, the association of DEAD box RNA helicase Ddx17 with *Myoparr* was of interest, because Ddx17 was shown to be required for myogenesis [22,23]. We thus investigated the role of Ddx17 in *Myoparr*-mediated transcriptional activation. Specific association of *Myoparr* with endogenous Ddx17 was confirmed by *Myoparr* immunoprecipitation followed by immunoblotting with a Ddx17-specific antibody (Fig 4B). In addition, the 341-nt region of *Myoparr* was shown to be required for binding with Ddx17 by RNA pull-down experiments (Fig 4C). Furthermore, intracellular binding between endogenous *Myoparr* and Ddx17 was confirmed by RNA immunoprecipitation using a Ddx17-specific antibody and qRT–PCR (Appendix Fig S3B). These results indicated a direct interaction between *Myoparr* and Ddx17 and suggested the involvement of this interaction in *Myoparr*-mediated transcriptional activation.

The process of lncRNA transcription rather than lncRNA transcripts may contribute to neighboring gene regulation [24]. We then determined whether *Myoparr* transcription or *Myoparr* transcript is required for the activation of *myogenin*. We showed that *Myoparr* depletion altered histone modifications at the *myogenin* locus (Fig 3D). Therefore, we cloned the upstream region of *myogenin* (−1649 to +52; containing *myogenin* promoter region and *Myoparr*, Fig 4D) into an episomal luciferase vector, which forms a proper chromatin structure [25], to create the −1650-Luc. In comparison with the −242-Luc (−242 to +52; containing *myogenin* promoter region but not *Myoparr*), the −1650-Luc showed 6.5-fold higher promoter activity, whereas insertion of *EGFP* instead of *Myoparr* (−242+EGFP-Luc) showed no increased activity in differentiating C2C12 cells (Fig 4E and Appendix Fig S3C). Deletion of the

Figure 3. *Myoparr* is required for the activation of *myogenin* and C2C12 differentiation.

A C2C12 cells were transfected with 50 nM of indicated siRNAs in growth medium. After additional 24-h incubation in growth medium, cells were transferred to differentiation medium. The levels of *Myoparr* and *myogenin* expression were quantified by qRT–PCR 24 h after differentiation induction. $n = 3$, mean ± SD. $^{*}P < 0.05$. n.s., not significant. Statistical analyses were performed using unpaired two-tailed Student's *t*-test (*Myoparr*; Cont1 *vs.* siRNA-1, *myogenin*; Cont1 *vs.* Cont2). In cases of unequal variances (*Myoparr*; Cont1 *vs.* Cont2 and Cont1 *vs.* siRNA-2, *myogenin*; Cont1 *vs.* siRNA-1 and Cont1 *vs.* siRNA-2), unpaired two-tailed Welch's *t*-test was used.

B Western blot showing decreased expression of myogenin in differentiating C2C12 cells 48 h after *Myoparr* KD. Tubulin expression served as an internal control.

C The expression levels of *myogenin* and *Myoparr* evaluated by qRT–PCR in *myogenin*-depleted C2C12 cells. $n = 3$, mean ± SD. $^{**}P < 0.01$. $^{***}P < 0.001$ (unpaired two-tailed Student's *t*-test).

D ChIP-qPCR detection of Pol II occupancy and histone modification status at the *myogenin* locus in *Myoparr*-depleted differentiating C2C12 cells. The data were normalized to input values. $n = 3$, mean ± SD. $^{*}P < 0.05$. $^{**}P < 0.01$ (unpaired two-tailed Student's *t*-test or unpaired two-tailed Welch's *t*-test).

E Retrieval rate of *Myoparr* using *Myoparr*-ChIRP probes from C2C12 cells quantified by qPCR is shown as percent of input values. *GAPDH* was amplified as a negative control. $n = 3$, mean ± SD. ND, not detected.

F ChIRP-qPCR detection of the interaction between endogenous *Myoparr* and the *myogenin* promoter. The *myogenin* 3′UTR and *GAPDH* promoter were amplified as negative controls. The data were normalized to input values. $n = 3$, mean ± SD. $^{*}P < 0.05$. $^{**}P < 0.01$ (unpaired two-tailed Welch's *t*-test). ND, not detected.

G, H Immunocytochemistry for the detection of myogenin at 24 h (G) or MHC at 72 h (H) in *Myoparr*-depleted C2C12 cells after differentiation induction. Nuclei were counterstained with DAPI. Scale bars, 100 μm. The percentage of myogenin-positive cells or fusion index is shown as percent of the control. $n = 3$, mean ± SD. $^{**}P < 0.01$ (unpaired two-tailed Welch's *t*-test). $^{***}P < 0.001$ (unpaired two-tailed Student's *t*-test).

I The intersection of genes regulated by *Myoparr* KD and *myogenin* KD shows a significant (Fisher's exact test) overlap 25.6 times as large as expected by chance alone.

J Genes significantly differentially expressed in both *Myoparr*- and *myogenin*-depleted cells show correlated expression ($R = 0.63$, log 2 ratio scale).

K–N Enrichment of GO categories in genes up-regulated by *Myoparr* KD (K), down-regulated by *Myoparr* KD (L), down-regulated by *myogenin* KD (M), and commonly regulated by both *Myoparr* KD and *myogenin* KD (N).

upstream region of *myogenin* (−1194 to −854), which corresponds to the Ddx17-binding region of *Myoparr* (612–952 in RNA), from the −1650-Luc greatly reduced the activity of the −1650-Luc (Fig 4F). The deleted region had no classical enhancer activity (Fig 4G), indicating the importance of the Ddx17-binding region of *Myoparr* for the activation of *myogenin* promoter. In accordance with these

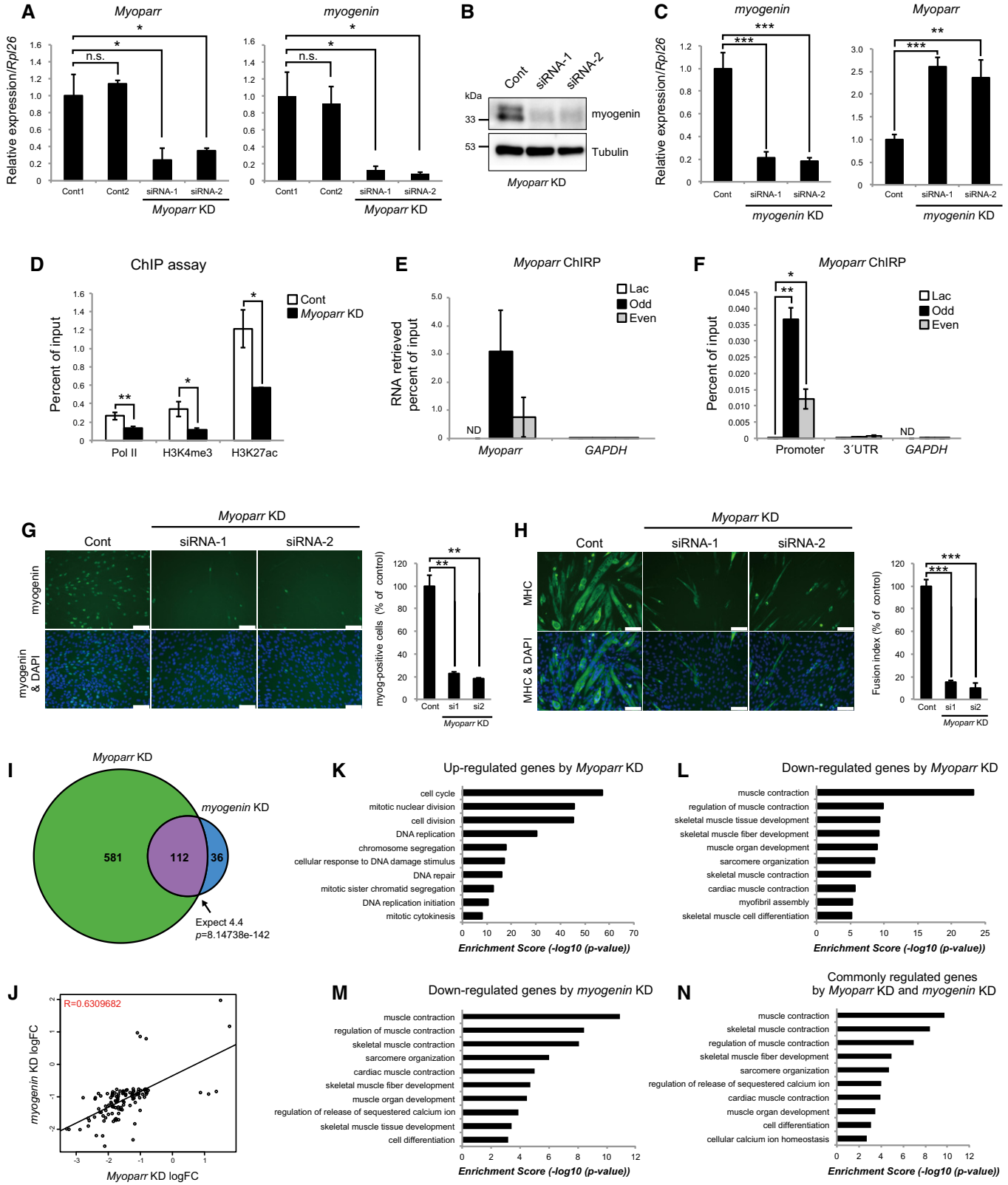

Figure 3.

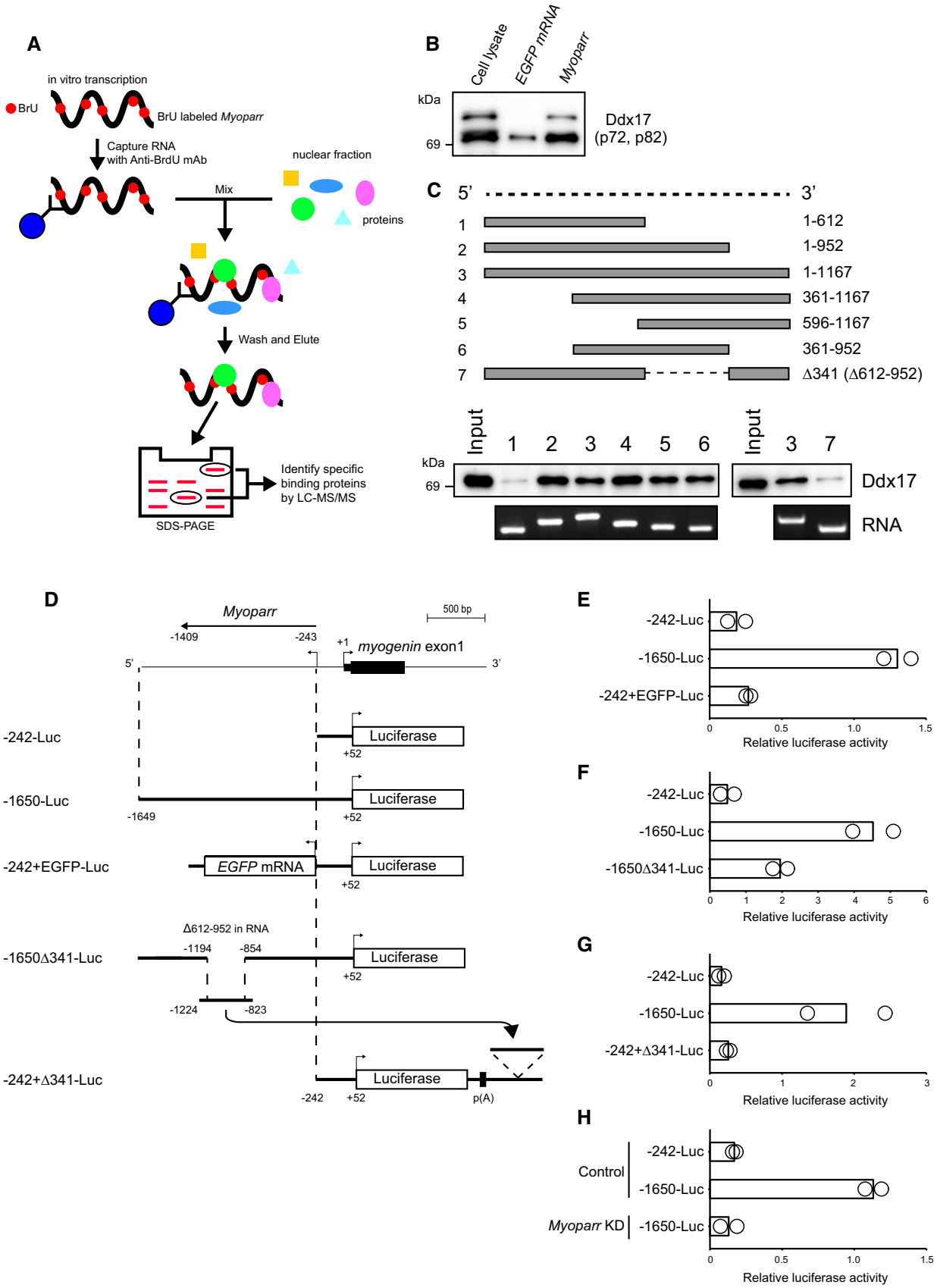

Figure 4.

Figure 4. *Myoparr* interacts with DEAD box protein Ddx17.

A Scheme of the identification of *Myoparr*-interacting proteins using RiboTrap and differential proteomics analysis.

B Following immunoprecipitation, the interaction between *Myoparr* and endogenous Ddx17 was confirmed by immunoblotting using a Ddx17-specific antibody. Two different Ddx17 isoforms (p72 and p82) were observed.

C Determination of the Ddx17-binding region of *Myoparr* by RNA pull-down analyses. Schematic diagram of full-length or truncated *Myoparr* used for RNA pull-down (top). *In vitro*-transcribed/*in vitro*-translated Ddx17 protein was pulled down by indicated *Myoparr* and then detected by Western blot using a Ddx17 antibody (bottom).

D Schematic diagram of the constructs used for luciferase assays. The details of all constructs are described in Materials and Methods. p(A) indicates poly(A) site.

E–G Relative luciferase activities of indicated constructs in differentiating C2C12 cells.

H Relative luciferase activities of indicated constructs in differentiating C2C12 cells transfected with control or *Myoparr* shRNA (*Myoparr* KD).

Data information: In (E-H), bars indicate the average of two independent experiments, and open circles represent the values of each experiment.

findings, elevated activity of the −1650-Luc was completely abolished by *Myoparr* KD in differentiating C2C12 cells (Fig 4H and Appendix Fig S3D). Thus, these results indicated that *Myoparr* transcript containing the Ddx17-binding region is crucial for *myogenin* activation.

Simultaneous depletion of *Ddx17* and highly related *Ddx5* inhibited C2C12 differentiation and the activation of myogenic genes including *myogenin* [22]. We found that depletion of *Ddx17* alone was sufficient to inhibit myogenic differentiation as shown by decreased MHC expression (Fig 5A and Appendix Fig S4A). Additionally, the expression of *myogenin* and *Myoparr* was significantly decreased in *Ddx17*-depleted cells (Fig 5B and Appendix Fig S4B and C). On the contrary, Ddx17 expression was increased by a small amount by either *Myoparr* or *myogenin* KD (Appendix Fig S4D). We showed that exogenous overexpression of Ddx17 with MyoD increased the activity of the −1650-Luc in C2C12 cells (Fig 5C). This synergistic activation was not observed in a Ddx17 mutant (K142R), which retains the *Myoparr*-binding activity but lacks the RNA helicase activity [26] (Fig 5D), suggesting that the helicase activity of Ddx17 could be indispensable for the activation of *myogenin* expression.

Ddx17 interacts with transcriptional regulators in C2C12 cells [22]. To reveal the mechanism by which *Myoparr* regulates the transcriptional activity of Ddx17 during myogenesis, we examined the effect of *Myoparr* depletion on these interactions by coimmunoprecipitation assays. Among these interactions, *Myoparr* depletion significantly decreased the interaction between Ddx17 and histone acetyltransferase PCAF in differentiating C2C12 cells (Fig 5E and F), indicating that *Myoparr* was required for the protein–protein interaction between Ddx17 and PCAF. Moreover, *in vitro* pull-down assay using 3xFlag-Ddx17 showed that the protein–protein interaction between Ddx17 and PCAF was augmented in the presence of *Myoparr* (Fig 5G). Although Ddx17 and PCAF directly bound to *myogenin* promoter, *Myoparr* was dispensable for these bindings (Fig 5H and I). Thus, these results suggested that *Myoparr* activates *myogenin* expression by promoting formation of the Ddx17-PCAF complex on the *myogenin* locus in differentiating myoblasts.

Myoparr and Ddx17 are required for myoblast cell cycle withdrawal in a *myogenin*-independent manner

To determine whether Ddx17 mediates the function of *Myoparr* in the cell cycle and cell division pathway, we compared the genes regulated by *Ddx17* KD and *Myoparr* KD by RNA-seq. Depletion of *Ddx17* increased expression of 93 genes and decreased expression of 204 genes in a statistically significant manner (Table EV1). Eighty percent of genes altered by *Ddx17* KD overlapped with genes regulated by *Myoparr* KD, and the intersection of these genes was 26.9-fold greater than that expected by chance ($P = 4.621241 \times 10^{-317}$; Fig 6A and B, and Table EV1), with a high correlation coefficient ($R = 0.94$; Fig 6C). Intriguingly, although genes down-regulated by *Ddx17* KD were enriched in muscle contraction and muscle development categories in GO terms, genes whose expression was up-regulated by *Ddx17* KD were preferentially classified as cell cycle and cell division categories, consistent with *Myoparr* KD (Figs 3K and 6D and E, Table EV1). Consequently, genes commonly regulated by both *Myoparr* KD and *Ddx17* KD (236 genes) were also enriched in the same categories (Fig 6F and Table EV1), suggesting that *Myoparr* and Ddx17 control the cell cycle withdrawal of proliferating myoblasts. Indeed, we observed a significant increase in 5-ethynyl-2′-deoxyuridine (EdU) incorporation in *Myoparr*- and *Ddx17*-depleted cells but not in *myogenin*-depleted cells (Fig 6G). These results indicated that *Myoparr* and Ddx17 regulate myoblast cell cycle withdrawal in a *myogenin*-independent manner.

To examine the mechanism by which *Myoparr* and Ddx17 regulate myoblast cell cycle withdrawal, we assessed the expression changes of genes categorized in GO terms: mitotic nuclear division, cell cycle, and cell division. Expression of *Rb1*, a negative regulator of cell cycle-promoting genes, was significantly decreased either by *Myoparr*, *Ddx17*, or *myogenin* depletion (Appendix Fig S5A). Nevertheless, the expression of many other cell cycle-promoting genes was maintained at a high level in *Myoparr*- and *Ddx17*-depleted cells but not in *myogenin*-depleted cells (Table EV1). Accordingly, we hypothesized that *Myoparr* KD or *Ddx17* KD might inhibit cell cycle withdrawal in an *Rb1*-independent manner. To test this hypothesis, we further analyzed the RNA-seq data and found that expression of the *miR-133b* primary transcript (*pri-miR-133b*) and *H19* was largely decreased either by *Myoparr* or *Ddx17* depletion but not by *myogenin* depletion (Fig 7A and Table EV1). In addition, the expression of *pri-miR-206*, located in the same cluster as *pri-miR-133b*, was specifically decreased by *Myoparr* or *Ddx17* KD (Fig 7A). To determine whether *Myoparr* regulates the expression of these miRNAs at the transcriptional level, we assessed the Pol II occupancy at these promoters by ChIP assays in *Myoparr*-depleted cells. As a result, *Myoparr* was required for the high level of Pol II occupancy at these promoters in differentiating C2C12 cells (Fig 7B). Regarding Ddx17 and PCAF, direct binding of Ddx17 and PCAF to these promoters was observed by ChIP assays, with the *GAPDH* locus as a negative control (Fig 7C and D). Intriguingly, *Myoparr* was dispensable for the binding of Ddx17 to these loci, and *Myoparr* KD increased PCAF occupancy at these promoters, suggesting that

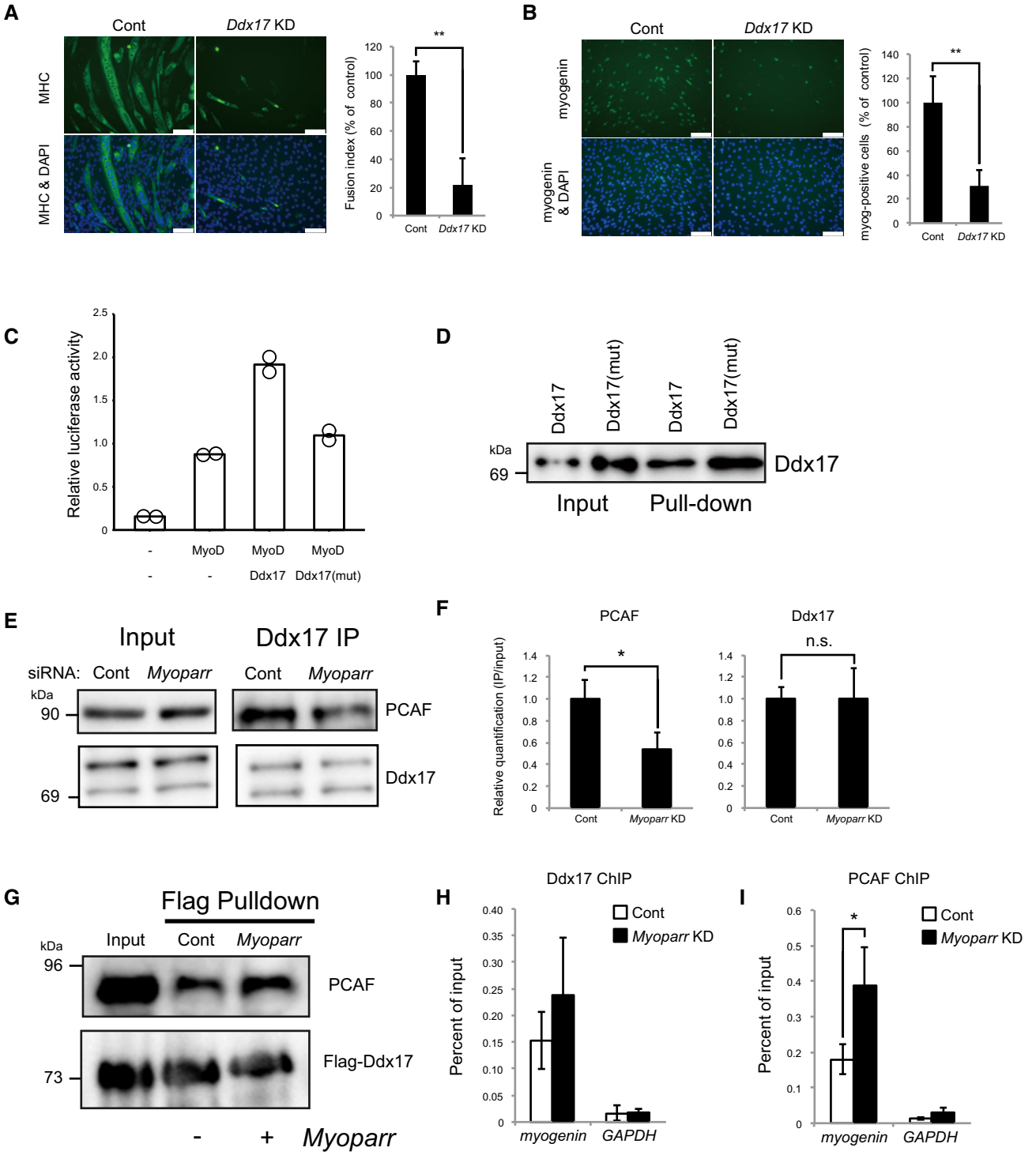

Figure 5.

occupancies of both Ddx17 and PCAF are not sufficient for maximum Pol II recruitment to target loci.

During C2C12 myogenesis, *miR-133b* down-regulates the phosphorylation of ERK1/2 to inhibit myoblast proliferation [27]. Inhibition of DNA synthesis through the down-regulation of DNA pol α (*Pola1*) at the mRNA level by *miR-206* facilitates myoblast cell cycle withdrawal [28]. *H19* inhibits the expression of cell cycle-related genes by targeting Cdc6, a member of the DNA replication initiation complex [29]. We observed significant decreases in the mature *miR-133b* and *miR-206* products in both *Myoparr*- and *Ddx17*-depleted cells (Fig 7E). Levels of mature *H19*-derived miRNAs, *miR-675-5p* and *miR-675-3p*, also tended to decrease (Appendix Fig S5B and C).

Figure 5. *Myoparr* promotes the protein–protein interaction between Ddx17 and PCAF.

A Significantly decreased MHC expression in *Ddx17*-depleted C2C12 cells is shown by immunocytochemistry. Nuclei were counterstained with DAPI. Scale bar, 100 μm. Fusion index is shown as percent of the control. $n = 3$, mean ± SD. $^{**}P < 0.01$ (unpaired two-tailed Student's *t*-test).

B Immunocytochemistry for myogenin in *Ddx17*-depleted C2C12 cells. Scale bar, 100 μm. Myogenin-positive cells are shown as percent of the control. $n = 4$, mean ± SD. $^{**}P < 0.01$ (unpaired two-tailed Student's *t*-test).

C Relative luciferase activities of the -1650-Luc by the combination of MyoD and Ddx17 or Ddx17 mutant (K142R). Bars indicate the average of two independent experiments, and open circles represent the values of each experiment.

D Ddx17 or Ddx17 mutant (K142R) was pulled down by full-length *Myoparr* and then detected by Western blot.

E Reduced interaction between endogenous Ddx17 and PCAF in *Myoparr*-depleted C2C12 cells. After *Myoparr* KD, the cell lysates were subjected to immunoprecipitation (IP) with a Ddx17-specific antibody 36 h after differentiation induction (right panel). Each lysate was loaded as an input (left panel).

F Relative quantification of (E) is shown as IP/input ratio. $n = 3$, mean ± SD. $^{*}P < 0.05$. n.s., not significant (unpaired two-tailed Student's *t*-test).

G Increased interaction between Ddx17 and PCAF by *Myoparr*. PCAF protein was pulled down by 3xFlag-Ddx17 in the presence or absence of *Myoparr* using a Flag antibody and then detected by Western blot.

H, I ChIP-qPCR detection of Ddx17 (H) and PCAF (I) occupancies at the *myogenin* locus in *Myoparr*-depleted differentiating C2C12 cells. The data were normalized to input values. $n = 3$, mean ± SD. $^{*}P < 0.05$ (unpaired two-tailed Student's *t*-test).

On the other hand, *miR-1*, one of the myogenic miRNAs, tended to decrease in all three KD samples (Appendix Fig S5D and E). We specifically observed increased ERK1/2 phosphorylation (pERK1/2) and Cdc6 expression in both *Myoparr*- and *Ddx17*-depleted cells (Fig 7F). The expression level of *Pola1* was also increased either by *Myoparr* or *Ddx17* depletion but not by *myogenin* depletion (Fig 7G). These results indicated that *Myoparr* and Ddx17 are required for myoblast cell cycle withdrawal through the activation of myogenic miRNA expression.

Myoparr is required for *myogenin* expression during denervation-induced skeletal muscle atrophy *in vivo*

Endogenous *myogenin* expression is repressed during skeletal muscle maturation by innervation [30]; however, *myogenin* expression is reactivated by denervation, leading to skeletal muscle atrophy [31]. To test the possibility that *Myoparr* is required for *myogenin* expression *in vivo*, we examined the role of *Myoparr* during denervation-induced muscle atrophy in adult mouse. Sciatic nerve transection significantly reduced tibialis anterior (TA) muscle mass (Figs 8A and EV4A), with increased *Myoparr* as well as *myogenin* expression (Figs 8B and C, and EV4B and C). For *in vivo* KD, *Myoparr*-specific shRNA sequences were examined in NIH3T3 cells (Fig EV4D). Electroporation-mediated transfer of *Myoparr* shRNA3 into the innervated TA muscles effectively knocked down endogenous *Myoparr* expression and significantly decreased *myogenin* expression (Fig EV4E). Remarkably, *Myoparr* KD substantially repressed the myogenin expression induced by denervation in TA muscles (Fig 8D), indicating that *Myoparr* is required for the activation of *myogenin* expression *in vivo*.

We finally examined whether *Myoparr* depletion prevents neurogenic atrophy in mice. Analyses of the innervated and denervated TA muscles transfected with *Myoparr* shRNA3 showed that *Myoparr* KD increased the denervated TA muscle weight by 20% compared with that of muscles transfected with control vector (25.8 ± 0.82 mg vs. 31.0 ± 0.71 mg, $P < 0.001$; Fig 8E) but not innervated TA muscle weight (37.2 ± 0.82 mg vs. 38.8 ± 0.96 mg, $P = 0.195$). Cross-sectional area (CSA) analysis of emerald green fluorescent protein (EmGFP)-positive *Myoparr* shRNA3-transfected myofibers demonstrated that *Myoparr* KD significantly increased the myofiber size of denervated TA muscles compared with that of muscles transfected with control vector (1,324.3 ± 81.4 μm^2 vs. 1,743.5 ± 85.4 μm^2, $P < 0.01$) (Fig 8F and G), whereas no significant difference was observed in the myofiber size of innervated TA muscles (2,112.9 ± 184.7 μm^2 vs. 2,188.2 ± 122.1 μm^2, $P = 0.714$), indicating that *Myoparr*-depleted myofibers showed resistance to denervation-induced muscle atrophy. Quantification of the fiber areas of individual transfected myofibers is shown in Fig EV4F and G. Thus, *Myoparr* may be a promising therapeutic target for skeletal muscle atrophy caused by denervation.

Discussion

Spatiotemporal expression of *myogenin* is controlled by multiple regulatory factors via the evolutionally conserved proximal promoter region [13]. In this study, we provide new insight into the regulatory mechanism underlying *myogenin* expression by identification and characterization of a novel promoter-associated lncRNA, *Myoparr*. During skeletal muscle differentiation, *Myoparr* is expressed from the upstream region of *myogenin*, corresponding to the sequences required for high-level *myogenin* expression in mice [14]. Our findings demonstrated that *Myoparr* is essential for the activation of *myogenin* expression by regulating the Pol II occupancy and histone modifications at the *myogenin* locus through

Figure 6. *Myoparr* and Ddx17 regulate myoblast cell cycle withdrawal in a *myogenin*-independent manner.

A Heatmap displaying expression changes of 754 genes significantly altered either in *Myoparr*- or *Ddx17*-depleted cells (log 2 ratio scale).

B The intersection of genes regulated by *Myoparr* KD and *Ddx17* KD shows a significant (Fisher's exact test) overlap 26.9 times as large as that expected by chance alone.

C Genes significantly differentially expressed in both *Myoparr*- and *Ddx17*-depleted cells show correlated expression ($R = 0.94$, log 2 ratio scale).

D–F Enrichment analysis of GO categories in genes up-regulated by *Ddx17* KD (D), down-regulated by *Ddx17* KD (E), and commonly regulated by both *Myoparr* KD and *Ddx17* KD (F).

G *Myoparr* and Ddx17 are required for C2C12 cell cycle withdrawal. C2C12 cells transfected with each siRNA were cultured in growth medium for 24 h. After differentiation induction, cells were maintained in differentiation medium for 40 h and then treated with EdU for 6 h. EdU-positive cells are shown as percent of the control. Nuclei were counterstained with Hoechst 33342. $n = 3$, mean ± SD. $^{**}P < 0.01$ (unpaired two-tailed Student's *t*-test). Scale bar, 100 μm.

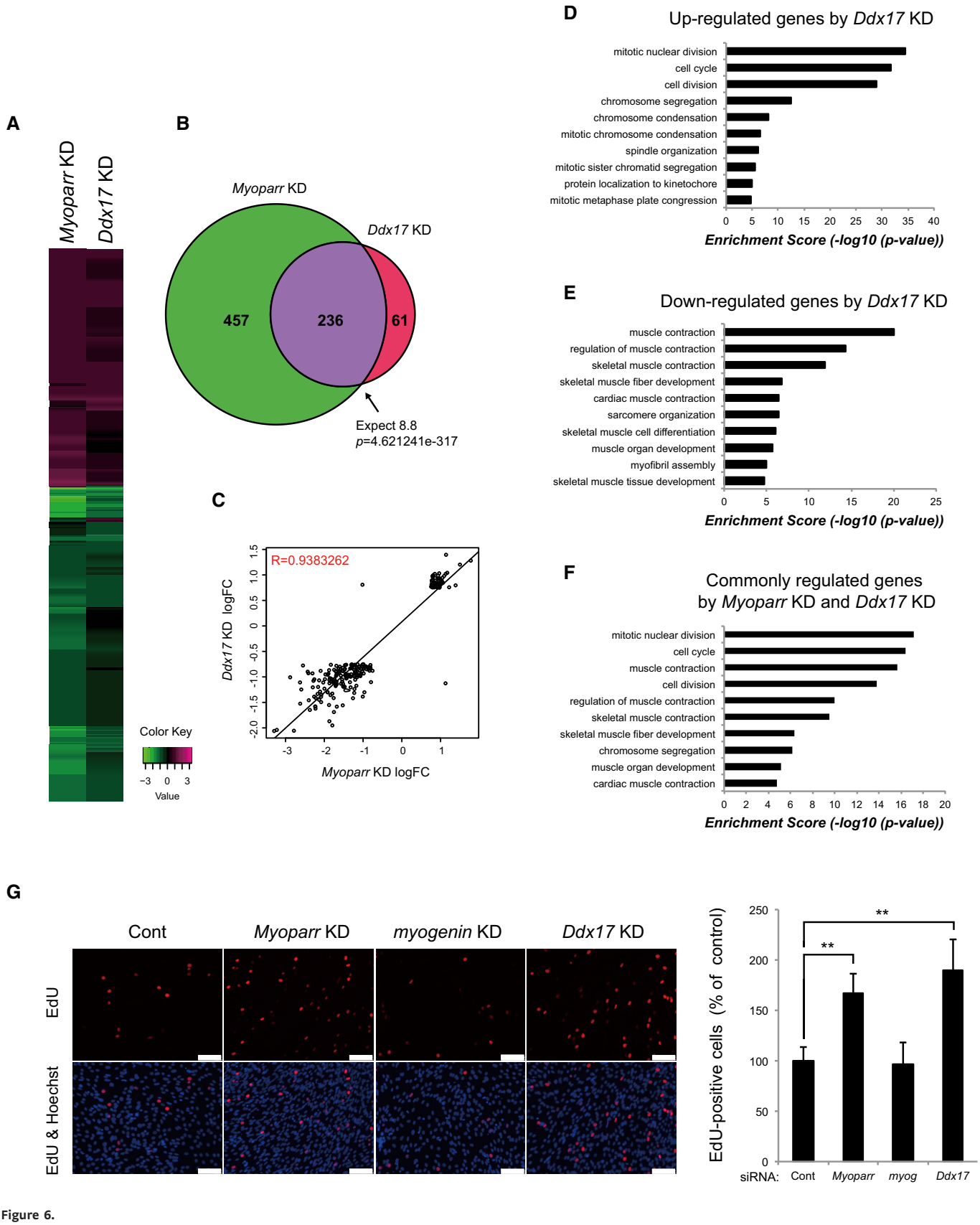

Figure 6.

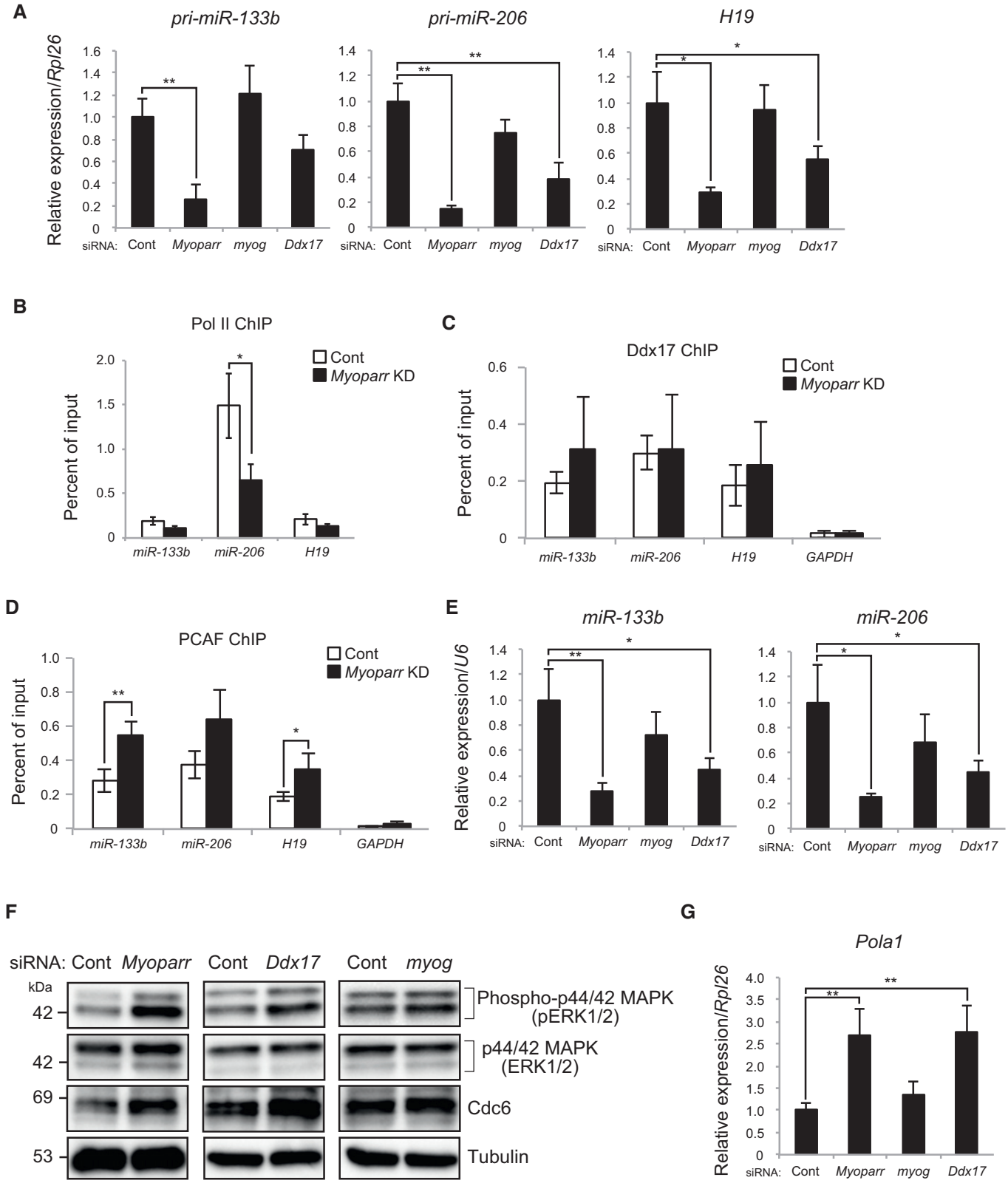

Figure 7.

binding to chromatin. Myogenin promotes the entry of myoblasts into the myogenic differentiation lineage [11]. Thus, *Myoparr* is required for the specification of myoblast lineage into myogenic differentiation through the *Myoparr* (upstream) and *myogenin* (downstream) pathway. In addition, we detected decreased expression of *miR-133b*, *miR-206*, and *H19*, regulators of myoblast

Figure 7. *Myoparr* regulates myoblast cell cycle withdrawal through the activation of *miR-133b*, *miR-206*, and *H19* expression.

A qRT–PCR for *pri-miR-133b*, *pri-miR-206*, and *H19* expression in differentiating C2C12 cells transfected with indicated siRNAs. $n = 3$, mean ± SD. $^{*}P < 0.05$. $^{**}P < 0.01$.

B ChIP-qPCR detection of Pol II occupancy at the indicated promoters in *Myoparr*-depleted C2C12 cells. The data were normalized to input values. $n = 3$, mean ± SD. $^{*}P < 0.05$. *Myoparr* KD decreased Pol II occupancy at the *miR-133b* promoter with a marginal trend toward significance ($P = 0.052$).

C, D ChIP-qPCR detection of Ddx17 (C) and PCAF (D) occupancies at the indicated promoters in *Myoparr*-depleted C2C12 cells. $n = 3$, mean ± SD. $^{*}P < 0.05$. $^{**}P < 0.01$.

E qRT–PCR showing decreased expression of *miR-133b* and *miR-206* in both *Myoparr*- and *Ddx17*-depleted C2C12 cells. $n = 3$, mean ± SD. $^{*}P < 0.05$. $^{**}P < 0.01$.

F Western blots showing increased ERK1/2 activity (pERK1/2) and Cdc6 expression in differentiating C2C12 cells 48 h after *Myoparr* and *Ddx17* KD. Tubulin expression served as an internal control.

G Increased *Pola1* expression detected by qRT–PCR. $n = 3$, mean ± SD. $^{**}P < 0.01$.

Data information: Statistical analyses were performed using unpaired two-tailed Student's *t*-test. In cases of unequal variances, unpaired two-tailed Welch's *t*-test was used.

proliferation [27–29], in *Myoparr*-depleted cells but not in *myogenin*-depleted cells. *Myoparr* was required for Pol II recruitment to these promoters. Consequently, *Myoparr* depletion prevented myoblast cell cycle arrest by increasing ERK1/2 activity and Cdc6 and *Pola1* expression. Taken together, our study revealed the roles of promoter-associated lncRNA *Myoparr*; one role is specification of myoblasts to differentiation lineage by activating neighboring *myogenin* expression, and the other role is myoblast cell cycle withdrawal by activating the expression of myogenic regulatory miRNAs in a *myogenin*-independent manner.

The DEAD box protein Ddx17 plays key roles in transcription, miRNA processing, alternative splicing, and myogenic differentiation [22,23,32]. In the present study, we discovered a new feature of Ddx17 as a *Myoparr*-interacting protein. Both Ddx17 and *Myoparr* were essential for *myogenin* expression. Deletion of the 341-nt DNA sequence, which corresponds to the Ddx17-binding region of *Myoparr*, from the *myogenin* upstream region largely reduced the promoter activity of *myogenin*. In differentiating myoblasts, Ddx17 functions as a transcriptional coactivator of MyoD through association with histone acetyltransferases CBP, p300, and PCAF [22]. PCAF also promotes transcriptional activities of Ddx17 and MyoD [33–35]. Although *Myoparr* was dispensable for the binding of Ddx17 and PCAF to the *myogenin* locus in our ChIP experiments, we showed that *Myoparr* is required to augment the interaction between Ddx17 and PCAF proteins. In addition, *Myoparr* was required for maximum Pol II recruitment to the *myogenin* promoter. Taken together, we proposed a model of *Myoparr* function during myogenesis (Fig 9).

Besides *myogenin* expression, our comprehensive RNA-seq analyses revealed that *Myoparr* regulates the expression of myogenic miRNAs in a *myogenin*-independent manner during C2C12 differentiation. Although not all the genes regulated by *Myoparr* KD completely overlapped with the genes regulated by *Ddx17* KD, our findings suggested that the *myogenin*-independent role of *Myoparr* in myoblast cell cycle withdrawal is largely mediated by Ddx17. PCAF is also essential for myoblast cell cycle arrest [36]. It is of note that *Myoparr* was indispensable for maximum Pol II recruitment to myogenic miRNA promoters but was dispensable for Ddx17 and PCAF recruitment, suggesting that *Myoparr*-mediated Ddx17-PCAF interaction is necessary for the expression of myogenic miRNAs. However, the mechanism by which low-copy-number *Myoparr* regulates the expression of downstream genes at distal loci remains to be determined. Considering that RNAs can exert a chaperone-like effect on their binding proteins [37,38], it is possible that *Myoparr*, by acting as a molecular chaperone, is required for the spatiotemporal timing of Ddx17 interaction with PCAF at the *myogenin* locus but not required for the maintenance of the complex thereof. In fact, our immunoprecipitation experiments showed that *Myoparr* KD resulted in decreased amounts of Ddx17-PCAF complex, suggesting that *Myoparr* KD affected the amount of Ddx17-PCAF complex at the whole-cell level. Thus, *Myoparr* may regulate the expression of downstream genes by controlling the amount of Ddx17-PCAF complex at distal loci.

Two E-box elements in the *myogenin* promoter are important for the responsiveness of MyoD and TGF-β [20]. In this study, we found that *Myoparr* shares its promoter region with *myogenin* and that the introduction of mutations into the E-box elements in this region abolished activation of both promoters, possibly induced by endogenous MyoD. In addition, TGF-β-dependent repression of both

Figure 8. Knockdown of *Myoparr* blocks skeletal muscle atrophy caused by denervation in mice.

A Seven days after denervation, weights of innervated (–) and denervated (+) tibialis anterior (TA) muscles were measured. $n = 4$, mean ± SEM. $^{*}P < 0.05$ (unpaired two-tailed Student's *t*-test).

B Expression of *myogenin* in innervated and denervated TA muscles detected by qRT–PCR 7 days after denervation. $n = 4$, mean ± SD. $^{***}P < 0.001$ (unpaired two-tailed Welch's *t*-test).

C qRT–PCR showing increased *Myoparr* expression in denervated TA muscles 7 days after denervation. $n = 3$, mean ± SD. $^{***}P < 0.001$ (unpaired two-tailed Student's *t*-test).

D Immunoblot showing decreased expression of myogenin by *Myoparr* depletion in denervated TA muscles 7 days after denervation. Expression of tubulin served as an internal control.

E Weights of innervated and denervated TA muscles electroporated either with control or *Myoparr* shRNA. Muscle weights were measured 7 days after denervation. $n = 5$ for each group, mean ± SEM. $^{***}P < 0.001$. n.s., not significant (unpaired two-tailed Student's *t*-test).

F Representative immunostaining images for laminin (red) and EmGFP (green) of innervated or denervated TA muscles electroporated with control or *Myoparr* shRNA, both containing EmGFP. Scale bar, 100 μm.

G Cross-sectional area (CSA) of electroporated EmGFP-positive myofibers (250 fibers per sample) was analyzed 7 days after denervation. $n = 5$ for each group, mean ± SEM. $^{**}P < 0.01$. n.s., not significant (unpaired two-tailed Student's *t*-test).

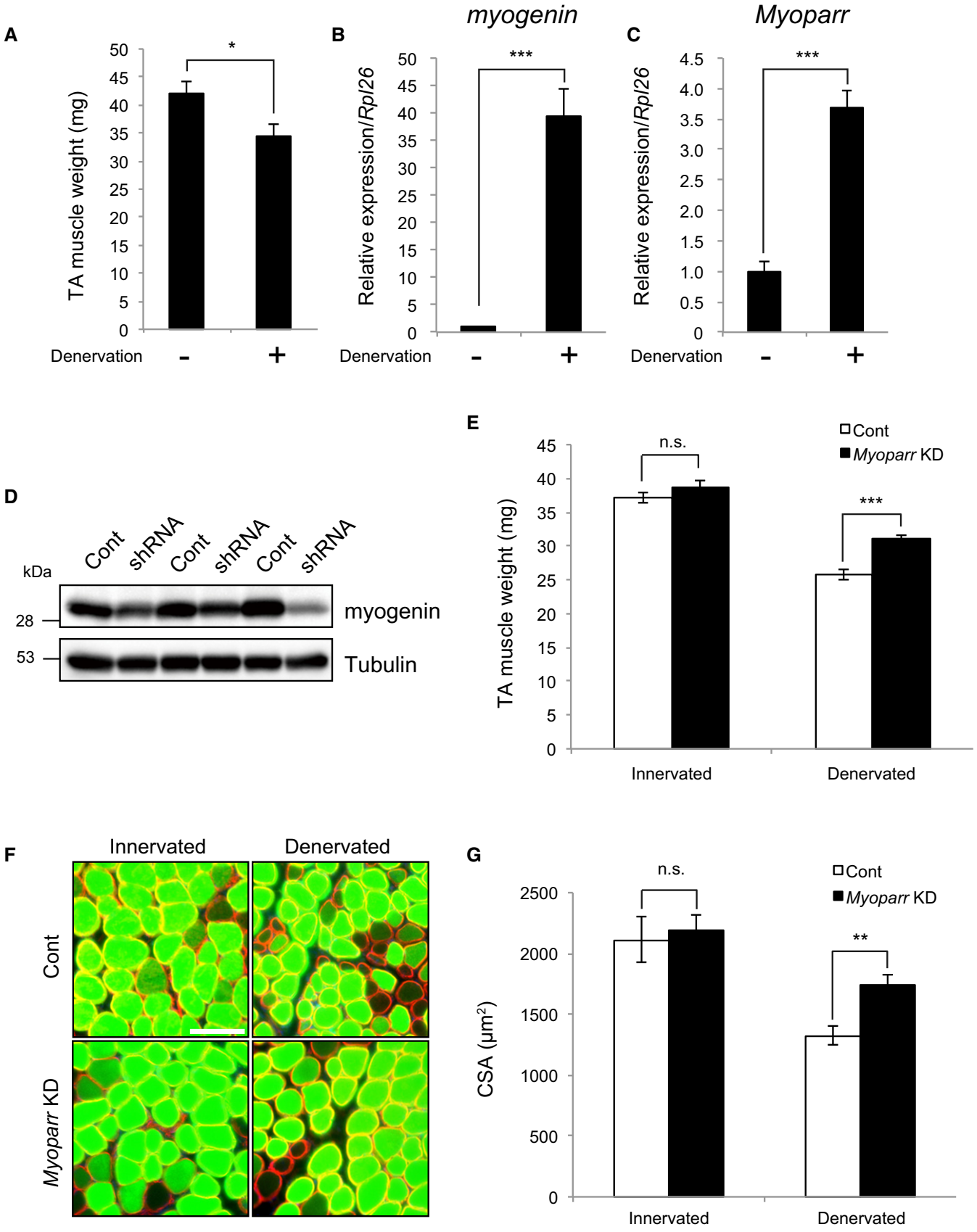

Figure 8.

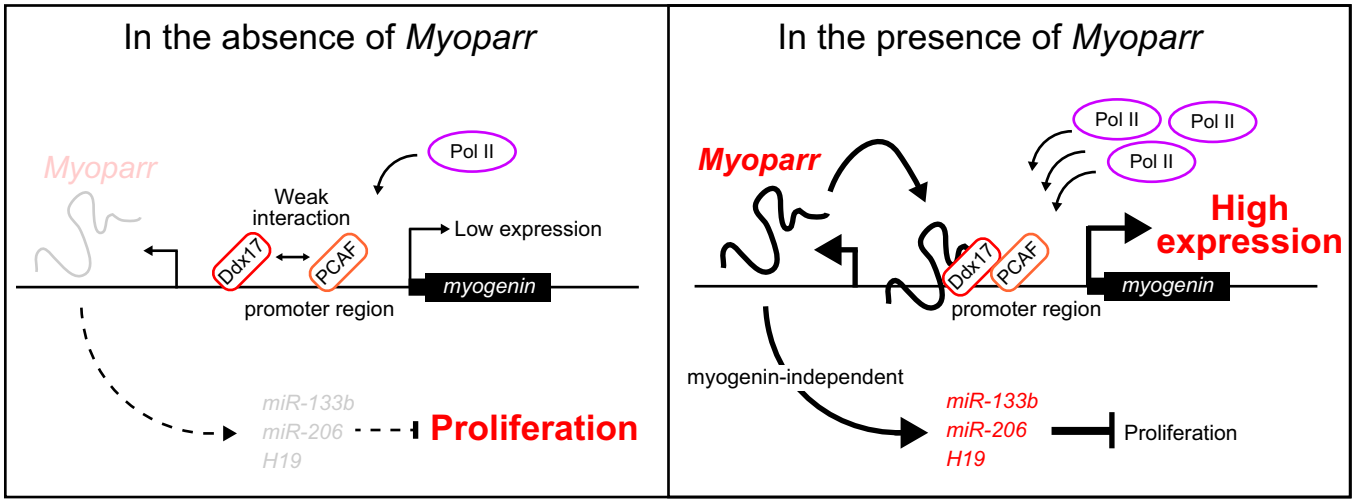

Figure 9. Proposed model of *Myoparr* function during myogenesis.
Although Ddx17 and PCAF bind to the *myogenin* promoter, the interaction between Ddx17 and PCAF is weak in the absence of *Myoparr*. Thus, occupancies of both Ddx17 and PCAF on the *myogenin* promoter are not sufficient for maximum Pol II recruitment to the *myogenin* promoter. After binding to the *myogenin* promoter, *Myoparr* interacts with Ddx17 to promote the Ddx17-PCAF interaction. Enhanced Ddx17-PCAF interaction by *Myoparr* may be sufficient for maximum Pol II recruitment to the *myogenin* promoter. Thus, *Myoparr* is required for specification of myoblast lineage into myogenic differentiation through the *Myoparr* (upstream) and *myogenin* (downstream) pathway. In addition, *Myoparr* is involved in the regulation of myoblast cell cycle withdrawal by activating the expression of myogenic regulatory miRNAs in a *myogenin*-independent manner.

promoter activities was attenuated by E-box mutations. Therefore, because multiple factors can be involved in *myogenin* regulation [13], common and intrinsic regulatory mechanisms may play a role in the expression of *Myoparr* and *myogenin*. Interestingly, *myogenin* KD increased *Myoparr* expression along with that of *Myf5* and *MRF4*, coding MyoD family MRFs. Up-regulated *Myf5* and *MRF4* expression was also reported in differentiating myoblasts derived from *myogenin* conditional knockout mice [39], suggesting that compensatory mechanisms induced by *myogenin* KD, i.e., increased expression of MyoD family MRFs, may increase *Myoparr* expression through the *myogenin/Myoparr* promoter.

After birth, innervation by motor neurons maintains the repressed status of *myogenin* expression in skeletal muscle [40]. When nerve supply to muscle is lost, *myogenin* expression is re-induced to promote proteolysis and atrophy in skeletal muscle [31]. In this study, we showed that *Myoparr* depletion led to down-regulation of myogenin expression re-induced by denervation and attenuated denervation-dependent reduction in skeletal muscle mass. Furthermore, we identified the human *Myoparr* counterpart and showed highly correlated expression of *myogenin* and *Myoparr* during human skeletal muscle differentiation. Besides denervation, re-induced *myogenin* expression has been reported in neurogenic atrophy, amyotrophic lateral sclerosis (ALS), Huntington's disease, and spinal muscular atrophy (SMA) [41–43]. Thus, our findings suggested that *Myoparr* inhibition may be a useful therapeutic strategy for neurogenic atrophy in humans.

In conclusion, we identified a novel promoter-associated lncRNA, *Myoparr*, and revealed its roles during myogenesis through the regulation of neighboring *myogenin* expression by promoting the protein–protein interaction between transcriptional activators. In addition, *Myoparr* was required for the expression of myogenic regulatory miRNAs in a *myogenin*-independent manner. Thus, our findings indicated that the promoter-associated lncRNA does not merely regulate neighboring gene expression but may also affect gene expression at distal loci in a neighboring gene-independent manner. However, we did not exclude the possibility that *Myoparr* may function independently through interaction of *myogenin* and Ddx17/PCAF proteins in myogenesis, because the genes affected by *Myoparr* KD did not completely overlap with those affected by *myogenin* or *Ddx17* KD. Besides Ddx17, we identified hnRNPK and Tial1, key interactors of lncRNA regulating the p53 pathway [44,45], as *Myoparr*-interacting proteins. Collectively, future studies using comprehensive analysis of *Myoparr*-interacting proteins will further define the roles of *Myoparr* in skeletal muscle formation and disorders affecting muscles.

Materials and Methods

Mouse model

The C57BL/6J mice used in this study were purchased from the Japan SLC and housed in cages with a constant temperature (24°C) and a 12:12-h light–dark cycle. All animal experiments were conducted under protocols approved by the Institutional Animal Care and Use Committee of Fujita Health University.

Cell lines and primary cultures

Mouse myoblast cell line, C2C12, was purchased from Marinpharm. NIH3T3 and C3H10T1/2 cells were purchased from the American Type Culture Collection (ATCC). C2C12 and NIH3T3 cells were maintained in Dulbecco's modified Eagle's medium (DMEM) supplemented with 10% fetal bovine serum at 37°C and 5% CO_2. Mouse embryonic fibroblast C3H10T1/2 cells were maintained in Eagle's minimum essential medium, alpha modification (α-MEM)

supplemented with 10% fetal bovine serum and 2 mM L-glutamine at 37°C and 5% CO_2. Myogenic differentiation was induced by replacing the medium with DMEM supplemented with 2% horse serum. For TGF-β treatment, C2C12 cells were cultured with 5 ng/ml recombinant TGF-β1 (R&D Systems) in DMEM supplemented with 2% horse serum for 24 h.

Mouse primary myoblasts were freshly prepared by FACS and cultured as previously described [46]. Myogenic differentiation of primary myoblasts was induced by replacing the medium with DMEM supplemented with 5% horse serum.

Experiments using human samples were approved by the Ethical Review Board for Clinical Studies at Fujita Health University. Gluteus medius muscles of patients undergoing total hip arthroplasty were used for cell preparation. Cells were sorted by FACS and cultured as previously described [47]. Human skeletal muscle myoblasts (HSMM) used for RACE analyses were purchased from Lonza and similarly isolated using FACS.

Plasmid DNA construction

The intergenic region between *Myoparr* and *myogenin* (−242/+51), including the minimal *myogenin* promoter region [14], was PCR-amplified and cloned into the pGL4.20 vector (Promega) in the positive or opposite direction to generate the pGL4-Myog-Luc (*myogenin* promoter) and pGL4-Myoparr-Luc (*Myoparr* promoter) constructs, respectively. Identified E-box elements in the intergenic region between *Myoparr* and *myogenin* [14] were mutated (CACATG to tgCAca and CAGTTG to tgGTca). The promoter region of mouse *GAPDH* (−560/+28) was PCR-amplified and cloned into the pGL4.20 vector in the positive or opposite direction to generate the *GAPDH* promoter constructs.

The upstream regions of the *myogenin* gene, −242/+51 and −1650/+51, were amplified by PCR and subcloned into the episomal luciferase vector, pREP4-luc, to generate the −242-Luc and −1650-Luc constructs, respectively. The coding region of *EGFP* was PCR-amplified and cloned into −242-Luc to generate the −242+EGFP-Luc construct. To create the −1650Δ341-Luc construct, the upstream region (−1194/−854) of the *myogenin* gene was removed from the −1650-Luc construct. The upstream region (−1224/−823) of the *myogenin* gene was PCR-amplified and inserted downstream of the poly(A) site in the −242-Luc construct to generate the −242 + Δ341-Luc construct. To create the pNL1.1-3xpA construct, the PGK promoter was removed from the pNL1.1.PGK vector (Promega) and the 3×poly(A) site amplified from the pRosa26-DEST vector was inserted upstream of Nluc.

The coding region of mouse *Ddx17* was PCR-amplified and subcloned into the pCS2+ and pCS2-3xFlag vectors. Mutant Ddx17 (K142R) was generated by PCR. The coding regions of *myogenin*, *PCAF*, and *EGFP* were PCR-amplified and subcloned into the pCS2+ vector. Full-length *Myoparr* and *myogenin*-associated sense long non-coding RNAs (short and long forms) were subcloned into the pCS2+ vector. Full-length and several indicated regions of *Myoparr* were PCR-amplified and cloned into the pGEM-T easy vector (Promega). The shRNA sequences against *Myoparr*, listed in Appendix Table S2, were subcloned into the pcDNA6.2-GW/EmGFP-miR vector (Thermo Fisher Scientific) according to the manufacturer's protocol. The pcDNA6.2-GW/EmGFP-miR containing the shRNA against *LacZ* (Thermo Fisher Scientific) was used as a negative control. The pcDNA3-MyoD construct has been previously described [48]. The pREP4-luc and pREP7-Rluc vectors were gifts from Dr. K. Zhao [25]. The pRosa26-DEST vector was a gift from Drs. N. Hastie and P. Hohenstein (Addgene plasmid # 21189) [49].

RNA and genomic DNA isolation, reverse transcription reaction, and PCR

Total RNA was prepared as previously described [48]. In brief, total RNA from tissues and cells was extracted and purified using the miRNeasy Mini Kit (QIAGEN) and ISOGEN II reagent (Nippon Gene, Japan) according to the manufacturer's protocol. To prepare total RNA from embryonic skeletal muscle, the trunk region of mouse embryos was surgically isolated at E10.5, E12.5, and E14.5. Embryonic organs were isolated at E14.5. Poly(A)+ RNAs were isolated from total RNA using the Poly(A)+ Isolation Kit (Nippon Gene) following the manufacturer's protocol. Nuclear and cytoplasmic RNA fractions were purified from C2C12 cells using the PARIS Kit (Thermo Fisher Scientific) according to the manufacturer's protocol. Nuclear fractionation (SNE and CPE) of C2C12 cells was performed as previously described [17]. Extraction of genomic DNA from C2C12 cells was performed using the PureLink Genomic DNA Kit (Thermo Fisher Scientific).

After treatment with DNase I (Thermo Fisher Scientific), the reverse transcription reaction was performed using the SuperScript III First-Strand Synthesis System with random or oligo (dT) primers (Thermo Fisher Scientific). A strand-specific reverse transcription reaction was performed as previously described [50] using the SuperScript III First-Strand Synthesis System with the indicated primers. For the analyses of miRNAs, cDNA was synthesized using the miScript Reverse Transcription Kit (QIAGEN). Semi-quantitative PCR analyses were conducted using Ex Taq (Takara) following the manufacturer's protocol. The quantitative real-time PCR was conducted using SYBR Premix Ex Taq (Takara) and the miScript SYBR Green PCR Kit (QIAGEN). Data were normalized to *Rpl26*, *GAPDH*, or *U6* expression as indicated. The primers used are listed in Appendix Table S3.

For semi-quantitative analyses, reverse transcription was performed on 1,000 ng RNA in a 20 μl reaction, and 1 μl cDNA was used for PCR in a 25 μl reaction volume for oligo (dT) priming as described above. When the reverse transcription was performed with strand-specific primers, 500 ng RNA was used in a 20 μl reaction, and 2 μl cDNA was used for PCR in a 25 μl reaction volume. PCR amplification was performed in 34 cycles using Ex Taq. We verified the PCR products by sequencing.

RNA-seq library construction, sequencing, and data analysis

Poly(A)+ RNAs were purified from 1 μg total RNA using the NEBNext Poly(A) mRNA Magnetic Isolation Module (New England Biolabs). RNA-seq libraries were constructed using the NEBNext Ultra RNA Library Prep Kit for Illumina (New England Biolabs) according to the manufacturer's protocol.

The libraries were sequenced with 100-bp single-end reads for each sample and two biological replicates per sample using an Illumina HiSeq 1500 at the Genome and Transcriptome Analysis Center of Fujita Health University. For basecalling, the bcl2fastq 1.8.4 software was used. Quality trimming of row sequence was performed

using FastQC ver. 0.11.3 software (https://www.bioinformatics.babraham.ac.uk/projects/fastqc/) following the command "-Q 33 -t 20 -l 30". Trimmed reads were aligned to the mouse reference genome (mm10) using Hisat2 ver. 2.0.5 [51] with default parameters. The number of aligned reads was approximately 95% of the original reads. Aligned reads were converted and sorted to Bam files using SAMtools ver. 1.3.1 software [52] and counted with HTSeq ver. 0.6.0 software [53] using the Mus_musculus_UCSC_mm10.gtf file following the optional command "–stranded = no –format = bam". Statistical analysis of differentially expressed genes was performed using DESeq2 ver. 1.12.4 software [54] with a Wald test (cut-offs: false discovery rate (adjusted *P*-value, padj) < 0.05 and log 2 fold change > 0.75 or < −0.75). GO analysis was performed with DAVID ver. 6.8 (https://david.ncifcrf.gov/), and $P < 0.005$ was considered statistically significant.

Absolute quantification of the copy numbers of *Myoparr* and *myogenin* RNA

The RNA copy numbers were quantified as previously described [55]. In brief, *Myoparr* and *myogenin* RNA (10^9 copies) was transcribed *in vitro* using the RiboMAX Large Scale RNA Production System (Promega) and was treated with DNase I then subjected to reverse transcription using the SuperScript III First-Strand Synthesis System with random primers. Synthesized cDNAs from *Myoparr* and *myogenin* RNA were serially diluted to be used as standards. Thirty-six hours after differentiation induction, total RNA was isolated from 5.45×10^5 C2C12 cells using the ISOGEN II reagent. One microgram of total RNA was treated with DNase I and subjected to reverse transcription. The copy numbers of endogenous *Myoparr* and *myogenin* RNA were quantified by qPCR, considering both the recovery rate of RNA and the ratio of myogenin-positive cells. The recovery rate of RNA during the RNA purification step was determined using *in vitro*-transcribed *EGFP* RNA (10^{12} copies) as a spike-in control. The ratio of myogenin-positive cells was determined by immunofluorescence analyses.

In vivo electroporation

For electroporation, the TA muscles of 8-week-old mice were injected with 30 μg endotoxin-free plasmid DNA in a saline solution using a 34-gauge needle under anesthesia. Electric pulses were applied with a tweezer-type electrode (150 V/cm, 6 pulses, 50 ms pulses of 1-Hz frequency) using a CUY21EDIT (Bex Co. LTD., Japan). Following electroporation, a 3-mm segment of the sciatic nerve was excised for denervation. Seven days after electroporation, mice were sacrificed and the TA muscles were fixed and immunostained as previously described [48]. Measurements of the CSA of the electroporated myofibers (EmGFP positive) were conducted with ImageJ software ver. 1.49.

siRNA treatment and immunofluorescence assay

C2C12 cells were transfected with 50 nM of Stealth RNAi (Thermo Fisher Scientific) or ASO (Takara) using Lipofectamine 3000 (Thermo Fisher Scientific) according to the manufacturer's protocol. The siRNAs used were as follows: Stealth RNAi siRNA negative controls (Med GC and Med GC Duplex #3) and siRNAs specific for *myogenin* (MSS275910 and MSS275912). The target sequences of the Stealth RNAi for *Myoparr* are as follows: 5′-GATGGACCCTGTCTGATGCTCTTAA-3′ and 5′-CCCTAAAGACCTACCACTACCACAT-3′. The Stealth RNAi for *Ddx17* was reported previously [22]. The target sequences of the ASO for *Myoparr* are as follows: 5′-CCATACTATGTCAGTC-3′ and 5′-TCTCTTCTGTGCTTTC-3′. The target sequences for the siRNA and shRNA used are listed in Appendix Table S2. Twenty-four hours after transfection, cells were induced for myogenic differentiation. Twenty-four hours or 72 h after differentiation induction, cells were collected for the analyses of RNAs and proteins.

Immunofluorescence analyses of C2C12 cells were performed as previously described [48]. Cells were fixed and stained with an anti-myogenin antibody (F5D, Developmental Studies Hybridoma Bank) on day 1, or with an anti-myosin heavy-chain antibody (MF20, Developmental Studies Hybridoma Bank) on day 3. EdU incorporation was assayed using the Click-iT Plus EdU Alexa Fluor 594 Imaging Kit (Thermo Fisher Scientific) according to the manufacturer's protocol. Nuclei were counterstained with DAPI or Hoechst 33342. Cells were visualized using a DMI4000B microscope (Leica) with a DFC350FX CCD camera (Leica) and then analyzed by ImageJ software ver. 1.49. The definition of the fusion index is the average number of nuclei in MHC-positive cells (at least three nuclei) per total nuclei number.

5′ and 3′ rapid amplification of cDNA ends (RACE)

RACE was performed using the GeneRacer Kit with the SuperScript III RT and TOPO TA Cloning Kit for Sequencing (Thermo Fisher Scientific) according to the instruction of the manufacturer. Poly (A)+ RNAs were used for the RACE reaction. Ex Taq and LA Taq with GC Buffer (Takara) were used for PCR amplification following the manufacturer's protocol. PCR products were gel purified with QIAquick (QIAGEN) and cloned into the pGEM-T easy vector then sequenced. The coding potential assessment was performed with a coding potential assessment tool (http://lilab.research.bcm.edu/cpat/) [56].

In vitro transcription and translation

In vitro transcription and translation were performed using the TnT SP6 High Yield Wheat Germ Protein Expression System (Promega) or TnT T7 Quick Coupled Transcription/Translation System (Promega) following the manufacturer's protocol. Ddx17 and 3xFlag-Ddx17 proteins were transcribed and translated using the TnT SP6 High Yield Wheat Germ Protein Expression System and then incubated in the TnT T7 Quick Coupled Transcription/Translation System with 45 mM ethylenediaminetetraacetic acid (EDTA). Proteins labeled with the FluoroTect GreenLys *in vitro* Translation Labeling System (Promega) were separated by SDS–PAGE and visualized with a Typhoon 9400 scanner (GE Healthcare).

Identification of *Myoparr*-binding proteins and the RNA pull-down assay

Myoparr-binding proteins were purified with the RiboTrap Kit (Medical & Biological Laboratories (MBL), Japan) according to the manufacturer's protocol. Briefly, 7×10^7 C2C12 cells were harvested 24 h

after myogenic induction and lysed in 1,200 μl CE Buffer containing 60 μl Detergent Solution. After centrifugation at 3,000 *g* for 3 min at 4°C, nuclei were washed three times with 1 ml CE Buffer and collected by centrifugation at 12,000 *g* for 3 min at 4°C. The nuclei were resuspended in 500 μl NE Buffer with sonication for 10 s. The nuclear lysate was diluted with 700 μl Dilution Buffer and centrifuged at 16,000 *g* for 10 min at 4°C. The supernatant was used for immunoprecipitation as the nuclear extract. The BrU-labeled *Myoparr* and *EGFP* RNA were prepared by the Riboprobe System (Promega). The BrU-labeled RNA (50 pmol) was bound to Protein G Plus Agarose (Thermo Fisher Scientific) conjugated to an anti-BrdU antibody and then mixed with the nuclear extract for 2 h at 4°C. RNA–protein complexes were washed four times with Wash Buffer I and then competitively eluted with 50 μl elution buffer containing free BrdU. Proteins were separated by SDS–PAGE, stained with SYPRO Ruby Protein Gel Stain (Thermo Fisher Scientific), and visualized with a Typhoon 9400 scanner. Representative bands specifically detected on the *Myoparr* sample were excised and in-gel digested with trypsin for analysis by mass spectrometry as previously described [57]. The peptide sequences obtained from the mass spectrometry analysis were searched against the protein database (Mass Spectrometry Sequence Database) using MASCOT software (Matrix Science).

An RNA pull-down assay was performed with the RiboTrap Kit and *in vitro*-transcribed/*in vitro*-translated Ddx17 protein. Various lengths of BrU-labeled *Myoparr* (10 pmol each) were bound to Protein G Plus Agarose conjugated to an anti-BrdU antibody and mixed with Ddx17 protein. After washing the RNA–protein complexes with Wash Buffer I, the Ddx17 protein was eluted and analyzed by Western blot.

RNA immunoprecipitation

Immunoprecipitation of endogenous RNAs was performed using the RIP-Assay Kit (MBL). In brief, 2×10^7 C2C12 cells were harvested 48 h after myogenic induction and lysed in 500 μl CE Buffer with 25 μl Detergent Solution. After centrifugation at 3,000 *g* for 3 min at 4°C, nuclei were washed three times with 400 μl CE Buffer and collected by centrifugation at 12,000 *g* for 3 min at 4°C. The nuclei were dissolved in 200 μl NE Buffer by Dounce homogenization (20 strokes) and then diluted with 300 μl Dilution Buffer. After centrifugation at 16,000 *g* for 10 min at 4°C, the supernatant was collected and mixed with Protein G Plus Agarose conjugated to the following antibodies: normal rabbit IgG (#2729S, Cell Signaling Technology (CST)) or Ddx17 antibody (N-13) (sc-86408, Santa Cruz Biotechnology (SCB)). After incubation with rotation for 3 h at 4°C, the beads were washed four times with Wash Buffer and the RNAs were eluted according to the manufacturer's protocol. Eluted RNAs were treated with DNase I, and the reverse transcription reaction was performed as described above. The precipitation percentage (precipitated RNA *vs*. input RNA) was calculated by qRT–PCR using the primers listed in Appendix Table S3.

Coimmunoprecipitation assay, protein pull-down assay, and Western blot analysis

For the coimmunoprecipitation assay, siRNA-treated C2C12 cells were maintained in DMEM supplemented with 2% horse serum. Cells were harvested 36 h after differentiation induction. Immunoprecipitation was performed by the two-step lysis method [58] using a Ddx17 antibody (S-17) (sc-86409, SCB).

An *in vitro* pull-down assay between 3xFlag-Ddx17 and PCAF protein was performed with the RiboTrap Kit with *in vitro*-transcribed/*in vitro*-translated proteins. The 3xFlag-Ddx17 protein was incubated with *Myoparr* or *EGFP* RNA (10 pmol each) then mixed with PCAF protein. Protein–RNA complexes were pulled down with an anti-Flag M2 Affinity Gel (A2220, Sigma-Aldrich) and analyzed by Western blot.

Western blot analyses were performed as previously described [48] with a minor modification. In brief, the samples were lysed in RIPA buffer (50 mM Tris–HCl (pH 8.0), 150 mM NaCl, 0.1% SDS, 1% Triton X-100, 0.5% sodium deoxycholate) containing protease inhibitors (1 mM phenylmethylsulfonyl fluoride, 1 μg/ml aprotinin, 4 μg/ml leupeptin) and phosphatase inhibitors (5 mM NaF, 5 mM β-glycerophosphate, 1 mM Na_3VO_4). Protein concentration was measured by the Pierce BCA Protein Assay Kit (Thermo Fischer Scientific), and equal amounts of protein were used for the Western blot analyses. The primary antibodies used for the Western blots are as follows: myogenin antibody (F5D) (sc-12732, SCB), MHC antibody (MF20, Developmental Studies Hybridoma Bank), Ddx17 antibody (N-13) (sc-86408, SCB), histone H2B antibody (07-371, Merck Millipore), p44/42 MAPK (ERK1/2) antibody (#9102, CST), phospho-p44/42 MAPK (pERK1/2) antibody (#4370, CST), Cdc6 (180.2) antibody (sc-9964, SCB), PCAF antibody (E-8) (sc-13124, SCB), α-tubulin antibody (#2144, CST), and Flag M2 antibody (F1804, Sigma-Aldrich). The HRP-linked secondary antibodies are as follows: anti-mouse IgG (#7076, CST), anti-rabbit IgG (#7074, CST), and Protein A-HRP (101023, Thermo Fisher Scientific). For the detection of PCAF, the PCAF antibody (E-8) was peroxidase-labeled by the Ab-10 Rapid Peroxidase Labeling Kit (Dojindo, Japan). Can Get Signal Immunoreaction Enhancer Solution (Toyobo, Japan) was used when necessary. All experiments were repeated at least twice.

Luciferase reporter assay

Subconfluent C2C12 cells were transfected with the indicated plasmids using Lipofectamine 2000 (Thermo Fisher Scientific). The total amount of DNA was kept constant by the addition of empty vectors when needed. As an internal control, pGL4.74 (Promega), pNL1.1.PGK, pREB7-Rluc, or pNL1.1-3xpA was used. Twenty-four hours later, myogenic induction was conducted as described above. Recombinant TGF-β1 was added if needed. Twenty-four hours after myogenic induction, cells were dissolved in Passive Lysis Buffer (Promega) to measure the indicated promoter-driven luciferase activities using a Lumat LB 9507 luminometer (Berthold Technologies) with the Dual-Luciferase Reporter Assay System (Promega) or Nano-Glo Dual-Luciferase Reporter Assay (Promega) according to the manufacturer's protocol. The promoter activity is presented as firefly to Renilla luciferase ratio or firefly to Nano luciferase ratio. The experiments were performed at least three times in duplicate or triplicate for each assay. Representative data are shown.

DNA methylation analysis

Genomic DNA (200 ng) was bisulfite treated using the Cells-to-CpG Bisulfite Conversion Kit (Thermo Fisher Scientific) according to the

manufacturer's protocol. The PCR was performed with EpiTaq HS (Takara) under the following conditions: denaturation at 94°C for 60 s and 35 cycles of 94°C for 30 s, 55°C for 30 s, and 72°C for 60 s. A second nested PCR was performed using the following conditions: denaturation at 94°C for 60 s and 25 cycles of 94°C for 30 s, 55°C for 30 s, and 72°C for 60 s. The primers used are listed in Appendix Table S3. The PCR products were subcloned into the pGEM-T easy vector, and clones derived from each independent subject ($n = 3$) were sequenced. The methylation status of the region (higher than 97% sequence identity) was determined and analyzed with QUMA (http://quma.cdb.riken.jp/top/quma_main_j.html).

Chromatin immunoprecipitation (ChIP) assay

For the ChIP assay, siRNA-treated C2C12 cells were maintained in DMEM supplemented with 2% horse serum. Thirty-six hours after differentiation induction, the cells were crosslinked with an N-hydroxysuccinimide-ester mixture (2 mM each of disuccinimidyl glutarate, disuccinimidyl suberate, and ethylene glycol-bis(succinic acid N-hydroxysuccinimide ester) in PBS) for 40 min at room temperature. After washing three times with PBS, cells were fixed with 1% formaldehyde for 15 min at room temperature and dissolved in ChIP lysis buffer (10 mM Tris–HCl (pH 8.0), 200 mM NaCl, 1 mM $CaCl_2$, 0.5% NP-40) containing protease inhibitors. Genomic DNA was sheared with Micrococcal Nuclease (1 unit/μl, Worthington Biochemical Corp.) for 10 min at 37°C. The shearing reaction was terminated by adding 2× SDS ChIP buffer (100 mM Tris–HCl (pH 8.0), 20 mM EDTA, 2% SDS, and protease inhibitors). The chromatin, containing approximately 10 μg DNA, was diluted (1:10) with ChIP dilution buffer (16.7 mM Tris–HCl (pH 8.0), 167 mM NaCl, 0.01% SDS, 1.1% Triton X-100, 1.2 mM EDTA) containing protease inhibitors then added to the ChIP reaction. Dynabeads M-280 sheep anti-rabbit IgG (Veritas) conjugated either with 2 μg Pol II antibody (39097, Active Motif), histone H3K4me3 antibody (39915, Active Motif), or histone H3K27ac antibody (39133, Active Motif) was used for the purification of the immunoprecipitated complex. If needed, 2 μg of the bridging antibody for mouse IgG (53017, Active Motif) was used.

For the Ddx17 and PCAF ChIP assays, siRNA-treated C2C12 cells were harvested 36 h after differentiation induction and crosslinked with 1% formaldehyde for 10 min at room temperature. After the reaction was quenched by glycine, cells were dissolved in NP-40 lysis buffer (10 mM Tris–HCl (pH 8.0), 200 mM NaCl, 1 mM $CaCl_2$, 0.5% NP-40, and protease inhibitors) and incubated on ice. After centrifugation at 7,300 *g* for 2 min at 4°C, nuclei were dissolved in SDS lysis buffer (50 mM Tris–HCl (pH 8.0), 10 mM EDTA (pH 8.0), 1% SDS, and protease inhibitors) and incubated on ice. To shear the genomic DNA, nuclear lysate diluted with Triton buffer (150 mM NaCl, 15 mM Tris–HCl (pH 8.0), 1 mM EDTA (pH 8.0), 1% Triton X-100, and protease inhibitors) was sonicated with a Bioruptor UCD-250 (Cosmo Bio, Japan) at the highest setting with 30-s ON, 30-s OFF pulse intervals for 30 cycles at 4°C. After confirming the fragmentation (100–500 bp in length), the lysate was centrifuged at 20,400 *g* for 10 min at 4°C, and the supernatant was used in the ChIP reaction. Dynabeads M-280 sheep anti-rabbit IgG conjugated to either 4 μg Ddx17 antibody (19910-1-AP, Proteintech) or PCAF antibody (E-8) was used to purify the immunoprecipitated complexes. If needed, 2 μg of the bridging antibody for mouse IgG was used.

Precipitates were sequentially washed in low-salt buffer (20 mM Tris–HCl (pH 8.0), 150 mM NaCl, 0.1% SDS, 1% Triton X-100, 2 mM EDTA), high-salt buffer (20 mM Tris–HCl (pH 8.0), 500 mM NaCl, 0.1% SDS, 1% Triton X-100, 2 mM EDTA), LiCl buffer (10 mM Tris–HCl (pH 8.0), 0.25 M LiCl, 1% NP-40, 1% sodium deoxycholate, 1 mM EDTA), and twice in TE buffer (10 mM Tris–HCl (pH 8.0), 1 mM EDTA). The immunoprecipitated complexes were extracted and de-crosslinked in ChIP direct elution buffer (10 mM Tris–HCl (pH 8.0), 300 mM NaCl, 0.5% SDS, 5 mM EDTA) at 65°C for 6–16 h. After sequential treatment with Ribonuclease (DNase free) Solution (Nippon Gene) at 37°C for 30 min and proteinase K (Takara) at 55°C for 1 h, DNA fragments were purified by NucleoSpin (Takara). The precipitation percentage (precipitated DNA *vs*. input DNA) was calculated by qPCR using the primers listed in Appendix Table S3.

Chromatin isolation by RNA purification assay

Chromatin isolation by RNA purification assays were performed following the protocol described by Chu *et al* [59]. In brief, C2C12 cells (3×10^7) harvested 36 h after differentiation induction were crosslinked with fresh 1% glutaraldehyde for 10 min at room temperature on an end-to-end rotator. The reaction was quenched by 0.1 volume of 1.25 M glycine at room temperature for 5 min. After washing with ice-cold PBS, the cells were lysed in lysis buffer (50 mM Tris–HCl (pH 7.0), 10 mM EDTA, 1% SDS, protease inhibitors, and SUPERase In RNase Inhibitor (1/200 volume, Thermo Fisher Scientific)) and sonicated with a Bioruptor UCD-250 at the highest setting with 30-s ON, 45-s OFF pulse intervals for 80 cycles at 4°C. After confirming the fragmentation (100–500 bp in length), the supernatant was hybridized with 100 pmol BiotinTEG-labeled tiling probes against *Myoparr* (Appendix Table S4) or *Lac*Z (Magna ChIRP Negative Control Probe Set, Merck Millipore) at 37°C for 4 h and then mixed with Dynabeads MyOne Streptavidin C1 (Veritas) at 37°C for 30 min. The beads were washed five times with Wash Buffer (0.5% SDS in 2× SSC) at 37°C for 5 min. The retrieved beads were used for following purifications (1/10 volume for RNA and 9/10 volume for DNA). The precipitation percentage (precipitated RNA or DNA *vs*. input RNA or DNA, respectively) was calculated by qPCR using the primers listed in Appendix Table S3.

Mapping of ChIP-seq data

Mapping of Pol II occupancy around the *myogenin* locus was performed using published ChIP-seq data. The data were downloaded from the Gene Expression Omnibus and converted into BigWig-formatted files using SraTailor software ver. 1.0.5 [60] on the mouse reference genome (mm9). The GEO accession code used for the analysis was GSE25549 [61].

Statistical analysis

Error bars represent SD unless otherwise indicated. Statistical analyses were performed using unpaired two-tailed Student's *t*-tests or unpaired two-tailed Welch's *t*-tests in cases of unequal variances. Statistical significance is reported in the Figures and Figure legends. $P < 0.05$ was considered statistically significant.

Data availability

The RNA-seq raw data for each sample reported in this paper were deposited into the DDBJ Sequence Read Archive under the accession No. DRA005527. The gene sequences reported in this paper were submitted to the DDBJ database. The accession numbers are as follows: AB921551 (*Myoparr* from the skeletal muscle of C57BL/6J), AB921552 (*Myoparr* from C2C12 cells), AB921553 (*myogenin*-associated sense long non-coding RNA isoform-1), AB921554 (*myogenin*-associated sense long non-coding RNA isoform-2), AB921556 (*myogenin*-associated sense long non-coding RNA isoform-3), AB921557 (*myogenin*-associated sense long non-coding RNA isoform-4), AB921555 (*myogenin*-associated sense long non-coding RNA isoform-5), LC388421 (*myogenin*-associated sense long non-coding RNA isoform-6), LC388422 (*myogenin*-associated sense long non-coding RNA isoform-7), LC366983 (human *Myoparr* isoform-1), and LC366984 (human *Myoparr* isoform-2).

Expanded View for this article is available online.

Acknowledgments
We thank Dr. H. Danno for technical advice. This work was supported in part by JSPS KAKENHI (25860151, 16K08599, and 17K08646), Intramural Research Grants (26-8 and 29-4) for Neurological and Psychiatric Disorders of NCNP, and a Grant-in-Aid from the NAKATOMI Foundation.

Author contributions
KH, MN, AT, YO, AU, HA, HI, and HK conducted the experiments. KH and KT designed the experiments and wrote the paper. All authors revised, edited, and read the manuscript and approved the final manuscript.

Conflict of interest
The authors declare that they have no conflict of interest.

References

1. Hon C-C, Ramilowski JA, Harshbarger J, Bertin N, Rackham OJL, Gough J, Denisenko E, Schmeier S, Poulsen TM, Severin J *et al* (2017) An atlas of human long non-coding RNAs with accurate 5' ends. *Nature* 543: 199 – 204
2. Andersson R, Gebhard C, Miguel-Escalada I, Hoof I, Bornholdt J, Boyd M, Chen Y, Zhao X, Schmidl C, Suzuki T *et al* (2014) An atlas of active enhancers across human cell types and tissues. *Nature* 507: 455 – 461
3. Luo S, Lu JY, Liu L, Yin Y, Chen C, Han X, Wu B, Xu R, Liu W, Yan P *et al* (2016) Divergent lncRNAs regulate gene expression and lineage differentiation in pluripotent cells. *Cell Stem Cell* 18: 637 – 652
4. Preker P, Nielsen J, Kammler S, Lykke-Andersen S, Christensen MS, Mapendano CK, Schierup MH, Jensen TH (2008) RNA exosome depletion reveals transcription upstream of active human promoters. *Science* 322: 1851 – 1854
5. Preker P, Almvig K, Christensen MS, Valen E, Mapendano CK, Sandelin A, Jensen TH (2011) PROMoter uPstream Transcripts share characteristics with mRNAs and are produced upstream of all three major types of mammalian promoters. *Nucleic Acids Res* 39: 7179 – 7193
6. Lepoivre C, Belhocine M, Bergon A, Griffon A, Yammine M, Vanhille L, Zacarias-Cabeza J, Garibal M-A, Koch F, Maqbool MA *et al* (2013) Divergent transcription is associated with promoters of transcriptional regulators. *BMC Genom* 14: 914
7. Sigova AA, Mullen AC, Molinie B, Gupta S, Orlando DA, Guenther MG, Almada AE, Lin C, Sharp PA, Giallourakis CC *et al* (2013) Divergent transcription of long noncoding RNA/mRNA gene pairs in embryonic stem cells. *Proc Natl Acad Sci USA* 110: 2876 – 2881
8. Hamazaki N, Uesaka M, Nakashima K, Agata K, Imamura T (2015) Gene activation-associated long noncoding RNAs function in mouse preimplantation development. *Development* 142: 910 – 920
9. Ruijtenberg S, van den Heuvel S (2016) Coordinating cell proliferation and differentiation: antagonism between cell cycle regulators and cell type-specific gene expression. *Cell Cycle* 15: 196 – 212
10. Tapscott SJ (2005) The circuitry of a master switch: myod and the regulation of skeletal muscle gene transcription. *Development* 132: 2685 – 2695
11. Cao Y, Kumar RM, Penn BH, Berkes CA, Kooperberg C, Boyer LA, Young RA, Tapscott SJ (2006) Global and gene-specific analyses show distinct roles for Myod and Myog at a common set of promoters. *EMBO J* 25: 502 – 511
12. Horak M, Novak J, Bienertova-Vasku J (2016) Muscle-specific microRNAs in skeletal muscle development. *Dev Biol* 410: 1 – 13
13. Faralli H, Dilworth FJ (2012) Turning on myogenin in muscle: a paradigm for understanding mechanisms of tissue-specific gene expression. *Comp Funct Genomics* 2012: 836374
14. Yee SP, Rigby PW (1993) The regulation of myogenin gene expression during the embryonic development of the mouse. *Genes Dev* 7: 1277 – 1289
15. Zhang B, Gunawardane L, Niazi F, Jahanbani F, Chen X, Valadkhan S (2014) A novel RNA motif mediates the strict nuclear localization of a long noncoding RNA. *Mol Cell Biol* 34: 2318 – 2329
16. Anderson KM, Anderson DM, McAnally JR, Shelton JM, Bassel-Duby R, Olson EN (2016) Transcription of the non-coding RNA upperhand controls Hand2 expression and heart development. *Nature* 539: 433 – 436
17. Werner MS, Ruthenburg AJ (2015) Nuclear fractionation reveals thousands of chromatin-tethered noncoding RNAs adjacent to active genes. *Cell Rep* 12: 1089 – 1098
18. Dimitrova N, Zamudio JR, Jong RM, Soukup D, Resnick R, Sarma K, Ward AJ, Raj A, Lee JT, Sharp PA *et al* (2014) LincRNA-p21 activates p21 in cis to promote Polycomb target gene expression and to enforce the G1/S checkpoint. *Mol Cell* 54: 777 – 790
19. Liu D, Kang JS, Derynck R (2004) TGF-beta-activated Smad3 represses MEF2-dependent transcription in myogenic differentiation. *EMBO J* 23: 1557 – 1566
20. Liu D, Black BL, Derynck R (2001) TGF-beta inhibits muscle differentiation through functional repression of myogenic transcription factors by Smad3. *Genes Dev* 15: 2950 – 2966
21. Fatica A, Bozzoni I (2014) Long non-coding RNAs: new players in cell differentiation and development. *Nat Rev Genet* 15: 7 – 21
22. Caretti G, Schiltz RL, Dilworth FJ, Di Padova M, Zhao P, Ogryzko V, Fuller-Pace FV, Hoffman EP, Tapscott SJ, Sartorelli V (2006) The RNA helicases p68/p72 and the noncoding RNA SRA are coregulators of MyoD and skeletal muscle differentiation. *Dev Cell* 11: 547 – 560
23. Dardenne E, Polay Espinoza M, Fattet L, Germann S, Lambert M-P, Neil H, Zonta E, Mortada H, Gratadou L, Deygas M *et al* (2014) RNA helicases DDX5 and DDX17 dynamically orchestrate transcription, miRNA, and splicing programs in cell differentiation. *Cell Rep* 7: 1900 – 1913
24. Engreitz JM, Haines JE, Perez EM, Munson G, Chen J, Kane M, McDonel PE, Guttman M, Lander ES (2016) Local regulation of gene expression by lncRNA promoters, transcription and splicing. *Nature* 539: 452 – 455
25. Liu R, Liu H, Chen X, Kirby M, Brown PO, Zhao K (2001) Regulation of CSF1 promoter by the SWI/SNF-like BAF complex. *Cell* 106: 309 – 318

26. Hönig A, Auboeuf D, Parker MM, O'Malley BW, Berget SM (2002) Regulation of alternative splicing by the ATP-dependent DEAD-box RNA helicase p72. *Mol Cell Biol* 22: 5698 – 5707
27. Feng Y, Niu L-L, Wei W, Zhang W-Y, Li X-Y, Cao J-H, Zhao S-H (2013) A feedback circuit between miR-133 and the ERK1/2 pathway involving an exquisite mechanism for regulating myoblast proliferation and differentiation. *Cell Death Dis* 4: e934
28. Kim HK, Lee YS, Sivaprasad U, Malhotra A, Dutta A (2006) Muscle-specific microRNA miR-206 promotes muscle differentiation. *J Cell Biol* 174: 677 – 687
29. Dey BK, Pfeifer K, Dutta A (2014) The H19 long noncoding RNA gives rise to microRNAs miR-675-3p and miR-675-5p to promote skeletal muscle differentiation and regeneration. *Genes Dev* 28: 491 – 501
30. Eftimie R, Brenner HR, Buonanno A (1991) Myogenin and MyoD join a family of skeletal muscle genes regulated by electrical activity. *Proc Natl Acad Sci USA* 88: 1349 – 1353
31. Moresi V, Williams AH, Meadows E, Flynn JM, Potthoff MJ, McAnally J, Shelton JM, Backs J, Klein WH, Richardson JA *et al* (2010) Myogenin and class II HDACs control neurogenic muscle atrophy by inducing E3 ubiquitin ligases. *Cell* 143: 35 – 45
32. Fuller-Pace FV (2013) The DEAD box proteins DDX5 (p68) and DDX17 (p72): multi-tasking transcriptional regulators. *Biochim Biophys Acta* 1829: 756 – 763
33. Sartorelli V, Puri PL, Hamamori Y, Ogryzko V, Chung G, Nakatani Y, Wang JY, Kedes L (1999) Acetylation of MyoD directed by PCAF is necessary for the execution of the muscle program. *Mol Cell* 4: 725 – 734
34. Dilworth FJ, Seaver KJ, Fishburn AL, Htet SL, Tapscott SJ (2004) *In vitro* transcription system delineates the distinct roles of the coactivators pCAF and p300 during MyoD/E47-dependent transactivation. *Proc Natl Acad Sci USA* 101: 11593 – 11598
35. Shin S, Janknecht R (2007) Concerted activation of the Mdm2 promoter by p72 RNA helicase and the coactivators p300 and P/CAF. *J Cell Biochem* 101: 1252 – 1265
36. Puri PL, Sartorelli V, Yang XJ, Hamamori Y, Ogryzko VV, Howard BH, Kedes L, Wang JY, Graessmann A, Nakatani Y *et al* (1997) Differential roles of p300 and PCAF acetyltransferases in muscle differentiation. *Mol Cell* 1: 35 – 45
37. Choi SI, Han KS, Kim CW, Ryu K-S, Kim BH, Kim K-H, Kim S-I, Kang TH, Shin H-C, Lim K-H *et al* (2008) Protein solubility and folding enhancement by interaction with RNA. *PLoS ONE* 3: e2677
38. Docter BE, Horowitz S, Gray MJ, Jakob U, Bardwell JCA (2016) Do nucleic acids moonlight as molecular chaperones? *Nucleic Acids Res* 44: 4835 – 4845
39. Meadows E, Cho J-H, Flynn JM, Klein WH (2008) Myogenin regulates a distinct genetic program in adult muscle stem cells. *Dev Biol* 322: 406 – 414
40. Méjat A, Ramond F, Bassel-Duby R, Khochbin S, Olson EN, Schaeffer L (2005) Histone deacetylase 9 couples neuronal activity to muscle chromatin acetylation and gene expression. *Nat Neurosci* 8: 313 – 321
41. Bricceno KV, Sampognaro PJ, Van Meerbeke JP, Sumner CJ, Fischbeck KH, Burnett BG (2012) Histone deacetylase inhibition suppresses myogenin-dependent atrogene activation in spinal muscular atrophy mice. *Hum Mol Genet* 21: 4448 – 4459
42. Galbiati M, Onesto E, Zito A, Crippa V, Rusmini P, Mariotti R, Bentivoglio M, Bendotti C, Poletti A (2012) The anabolic/androgenic steroid nandrolone exacerbates gene expression modifications induced by mutant SOD1 in muscles of mice models of amyotrophic lateral sclerosis. *Pharmacol Res* 65: 221 – 230
43. Mielcarek M, Toczek M, Smeets CJLM, Franklin SA, Bondulich MK, Jolinon N, Muller T, Ahmed M, Dick JRT, Piotrowska I *et al* (2015) HDAC4-myogenin axis as an important marker of HD-related skeletal muscle atrophy. *PLoS Genet* 11: e1005021
44. Huarte M, Guttman M, Feldser D, Garber M, Koziol MJ, Kenzelmann-Broz D, Khalil AM, Zuk O, Amit I, Rabani M *et al* (2010) A large intergenic noncoding RNA induced by p53 mediates global gene repression in the p53 response. *Cell* 142: 409 – 419
45. Liu L, Yue H, Liu Q, Yuan J, Li J, Wei G, Chen X, Lu Y, Guo M, Luo J *et al* (2016) LncRNA MT1JP functions as a tumor suppressor by interacting with TIAR to modulate the p53 pathway. *Oncotarget* 7: 15787 – 15800
46. Uezumi A, Fukada S-I, Yamamoto N, Takeda S, Tsuchida K (2010) Mesenchymal progenitors distinct from satellite cells contribute to ectopic fat cell formation in skeletal muscle. *Nat Cell Biol* 12: 143 – 152
47. Uezumi A, Fukada S, Yamamoto N, Ikemoto-Uezumi M, Nakatani M, Morita M, Yamaguchi A, Yamada H, Nishino I, Hamada Y *et al* (2014) Identification and characterization of PDGFRα+ mesenchymal progenitors in human skeletal muscle. *Cell Death Dis* 5: e1186
48. Hitachi K, Nakatani M, Tsuchida K (2014) Myostatin signaling regulates Akt activity via the regulation of miR-486 expression. *Int J Biochem Cell Biol* 47: 93 – 103
49. Hohenstein P, Slight J, Ozdemir DD, Burn SF, Berry R, Hastie ND (2008) High-efficiency Rosa26 knock-in vector construction for Cre-regulated overexpression and RNAi. *Pathogenetics* 1: 3
50. Hitachi K, Tsuchida K (2017) Myostatin-deficiency in mice increases global gene expression at the Dlk1-Dio3 locus in the skeletal muscle. *Oncotarget* 8: 5943 – 5953
51. Pertea M, Kim D, Pertea GM, Leek JT, Salzberg SL (2016) Transcript-level expression analysis of RNA-seq experiments with HISAT, StringTie and Ballgown. *Nat Protoc* 11: 1650 – 1667
52. Li H, Handsaker B, Wysoker A, Fennell T, Ruan J, Homer N, Marth G, Abecasis G, Durbin R, 1000 Genome Project Data Processing Subgroup (2009) The sequence alignment/Map format and SAMtools. *Bioinformatics* 25: 2078 – 2079
53. Anders S, Pyl PT, Huber W (2015) HTSeq–a Python framework to work with high-throughput sequencing data. *Bioinformatics* 31: 166 – 169
54. Love MI, Huber W, Anders S (2014) Moderated estimation of fold change and dispersion for RNA-seq data with DESeq2. *Genome Biol* 15: 550
55. Miao Y, Ajami NE, Huang T-S, Lin F-M, Lou C-H, Wang Y-T, Li S, Kang J, Munkacsi H, Maurya MR *et al* (2018) Enhancer-associated long non-coding RNA LEENE regulates endothelial nitric oxide synthase and endothelial function. *Nat Commun* 9: 292
56. Wang L, Park HJ, Dasari S, Wang S, Kocher J-P, Li W (2013) CPAT: coding-potential assessment tool using an alignment-free logistic regression model. *Nucleic Acids Res* 41: e74
57. Kurosawa G, Sumitomo M, Akahori Y, Matsuda K, Muramatsu C, Takasaki A, Iba Y, Eguchi K, Tanaka M, Suzuki K *et al* (2009) Methods for comprehensive identification of membrane proteins recognized by a large number of monoclonal antibodies. *J Immunol Methods* 351: 1 – 12
58. Klenova E, Chernukhin I, Inoue T, Shamsuddin S, Norton J (2002) Immunoprecipitation techniques for the analysis of transcription factor complexes. *Methods* 26: 254 – 259
59. Chu C, Quinn J, Chang HY (2012) Chromatin isolation by RNA purification (ChIRP). *J Vis Exp* 61: e3912
60. Oki S, Maehara K, Ohkawa Y, Meno C (2014) SraTailor: graphical user interface software for processing and visualizing ChIP-seq data. *Genes Cells* 19: 919 – 926
61. Mousavi K, Zare H, Wang AH, Sartorelli V (2012) Polycomb protein Ezh1 promotes RNA polymerase II elongation. *Mol Cell* 45: 255 – 262

